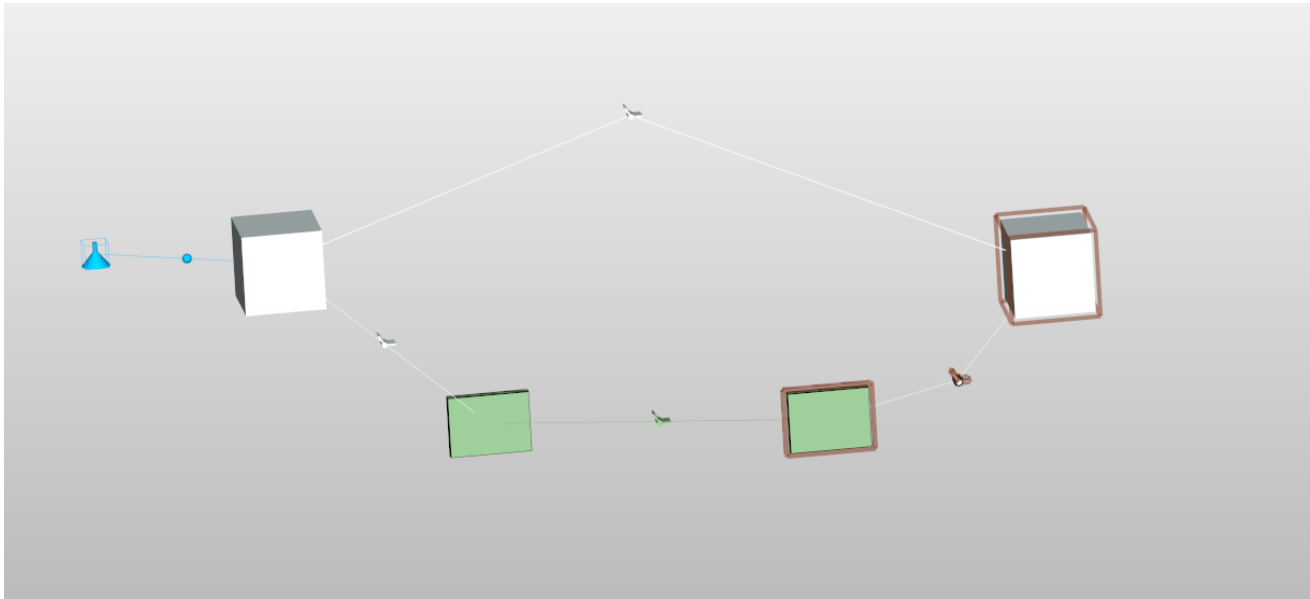




CHALMERS
UNIVERSITY OF TECHNOLOGY



Evaluating SEA modelling of lightweight building elements containing cross laminated timber

Master's thesis in the Master's Programme Sound and Vibrations

TOBIAS AUGUSTSSON

Department of Civil and Environmental Engineering
Division of Applied Acoustics

-
CHALMERS UNIVERSITY OF TECHNOLOGY
Gothenburg, Sweden 2016
Master's thesis BOMX02-16-151

MASTER'S THESIS BOMX02-16-151

Evaluating SEA modelling of lightweight building elements containing cross laminated timber

Master's thesis in the Master's Programme Sound and Vibrations

TOBIAS AUGUSTSSON

Department of Civil and Environmental Engineering
Division of Applied Acoustics

CHALMERS UNIVERSITY OF TECHNOLOGY

Gothenburg, Sweden 2016

Evaluating SEA modelling of lightweight building elements containing cross laminated timber
TOBIAS AUGUSTSSON

© TOBIAS AUGUSTSSON, 2016

Master's thesis BOMX02-16-151

ISSN 1652-8557

Department of Civil and Environmental Engineering

Division of Applied Acoustics

-

Chalmers University of Technology

SE-412 96 Gothenburg

Sweden

Telephone: +46 (0)31-772 1000

Cover:

SEAWOOD software workspace

Chalmers Reproservice

Gothenburg, Sweden 2016

Evaluating SEA modelling of lightweight building elements containing cross laminated timber
Master's thesis in the Master's Programme Sound and Vibrations

TOBIAS AUGUSTSSON

Department of Civil and Environmental Engineering
Division of Applied Acoustics

-

Chalmers University of Technology

ABSTRACT

To create a future sustainable environment more environmentally friendly building materials must be included in the building process. The use of timber is becoming more common when constructing larger dwellings. One of the challenges when using timber constructions is predicting the sound insulation. This thesis is a part of the project Silent Timber Build and aims to investigate the possibility of using statistical energy analysis (SEA) to predict sound insulation in timber buildings. The focus lies on a timber construction called cross laminated timber (CLT). SEA software has been developed by the French company, and Silent Timber Build partner, InterAC. This software, called SEAWOOD, is used to model the constructions investigated in this thesis. To get a better understanding of how the software operates, a simplified SEA model of a CLT plate is made in Matlab. To validate the SEA models the calculated reduction index curves are compared to lab measurements. These comparisons show that it is possible to model simpler timber constructions in SEA with reasonable accuracy. More complicated constructions may need more work to be properly modelled. Limitations in the SEA model makes it unsuitable for investigating the lower frequency region and other methods should be used to get more reliable results in this region.

Keywords: statistical energy analysis, SEA, cross laminated timber, CLT, modal overlap, modal density, Silent Timber Build, reduction index, sound insulation.

CONTENTS

Abstract	i
Contents	iii
Acknowledgements	v
1 Introduction	1
1.1 Background	1
1.2 General aim	1
1.3 Method / Outline	1
2 Theory	3
2.1 General SEA theory	3
2.1.1 Modes	5
2.2 CLFs	6
2.2.1 CLFs for structure-cavity interaction	6
2.2.2 CLFs for cavity-structure interaction	7
2.2.3 CLFs for structure-structure interaction	7
2.2.4 CLFs for direct transmission	7
2.3 Damping	8
2.4 Solving the power balance equations	9
2.5 SEAWOOD Theory	9
2.5.1 CLFs structure-cavity and cavity-structure	9
2.5.2 CLFs Direct transmission	9
2.5.3 CLFs for structure-structure interaction	10
2.5.4 Trim	11
2.5.5 Orthotropic Modal Thin Plate	11
2.5.6 Radiation efficiency	13
2.5.7 Uniform section, static and dynamic laminates	14
2.6 Simplified SEA model	15
3 SEAWOOD software	17
4 Estimating input data using parameter variation	19
5 Validation	25
5.1 Simplified SEA model	25
5.2 CLT140 floor between two rooms	25
5.2.1 Method	25
5.2.2 Results	27
5.3 CLT320 floor between two rooms	30

5.3.1	Method	30
5.3.2	Results	30
5.4	Assembly of CLT140 with impact sound insulation and Weber floor	33
5.4.1	Method	33
5.4.2	Results	34
5.5	Two CLT plates, mineral filled cavity, with and without added gypsum boards	37
5.5.1	Method	37
5.5.2	Results	39
5.6	CLT plate with foam insulation	43
5.6.1	Method	43
5.6.2	Results	43
5.7	CLT plate with foam insulation, mineral filled cavity and two gypsum boards.	47
5.7.1	Method	47
5.7.2	Results	48
5.8	CLT with a gypsum board separated by a mineral wool filled cavity and a added mineral wool insulation layer.	51
5.8.1	Method	51
5.8.2	Results	53
5.9	CLT between two cavities with mineral wool and CW and CD profiles and added gypsum boards	56
5.9.1	Method	56
5.9.2	Results	58
5.10	CLT and gypsum plates separated by a cavity filled with mineral wool and added CD profile	61
5.10.1	Method	61
5.10.2	Results	62
6	Discussion	64
7	Conclusion	66
	References	68
	Appendix A Appendix	69

ACKNOWLEDGEMENTS

I would like to thank the people behind the Silent Timber Build project, especially my supervisor Klas Hagberg, for making this thesis possible. I would also like to thank my supervisor at Chalmers, Jens Forssén, for all the helpful insight provided during this thesis. I was also fortunate to have met Jörgen Ohlsson from SP who provided helpful advise regarding the software and the modelling procedure.

1 Introduction

1.1 Background

This thesis is a part of the Silent Timber Build project. In the project a SEA software called SEAWOOD is refined and further developed in order to facilitate prediction of any wooden construction currently used in Europe. It might also be used in order to optimize future constructions in a wise manner based on modern requirements for wooden constructions. In this master thesis the software has been used to model a number of different floor and wall assemblies. All assemblies have been tested in an accredited laboratory in order to compare to the calculations. The calculations are primarily focused on airborne sound insulation. The wooden assemblies investigated in this thesis are plates made of cross laminated timber referred to as CLT. The CLT plates are made of single layer wood panels arranged at right angles to each other. These plates are then bonded together with glue. There CLT plates have different compositions depending on the thickness and amount of layers used in the construction. Figure 1.1 shows the general assembly of a CLT plate.



Figure 1.1: CLT plate. Figure from [14]

1.2 General aim

The aim of this thesis is to investigate the accuracy of the SEAWOOD software when modelling different kinds of assemblies including CLT plates. The aim is also to find out which parts of the modelling processes is most important to make accurate and believable calculations.

1.3 Method / Outline

The software SEAWOOD, which has been further developed within the research project Silent Timber Build, is a specific version of SEA+ provided by the French company InterAC. InterAC is research partner in Silent Timber Build. The software developed in the project has restricted mathematical libraries limited to plane elements and is dedicated to the wood building industry, to facilitate prediction of any wooden structure. Simulations have been carried out for airborne sound insulation levels. The

simulations presented here uses traditional SEA. All simulations are compared to the lab measurements of the constructions. All measurement data was made available by the project supervisor. The chosen timber constructions are intended to be used in the building process in the future. Due to secrecy regarding the exact measurements of some of the constructions, only the general assembly method are presented.

2 Theory

To try to emphasize how the software handles certain calculations the theory section are divided into three parts. These parts complement each other and should be seen only as separate parts if there is interest in how certain calculations are made for the different steps taken in this thesis.

2.1 General SEA theory

In SEA the average power flow between groups of coupled modes is proportional to the difference in the average modal energies. This makes it possible to investigate the response of a system that contains many resonant modes for a certain frequency range. This is done by dividing the structure into groups called subsystems and using a power balance equation for each subsystem. Figure 2.1 shows a model of the energy flow between two subsystems [1]

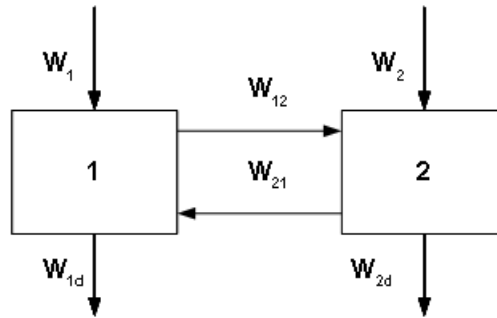


Figure 2.1: SEA model for two subsystems.

Energy flows to and from each subsystem. Each subsystem is excited by the power input into each system. W_1 and W_2 are power that is introduced into the system externally. W_{12} and W_{21} are energy that flows out of each subsystem due to transmission and radiation. Energy also flows out of the subsystems due to dissipations W_{1d} and W_{2d} . To fulfil a steady state condition the power going into a subsystem must be equal to the power that is flowing out of it. The power balance equation for the model in figure 2.1 are given in equations 2.1 and 2.2.

$$W_1 + W_{21} = W_{1d} + W_{12} \quad (2.1)$$

$$W_2 + W_{12} = W_{2d} + W_{21} \quad (2.2)$$

The dissipated energy in each subsystem is described by the internal loss factor η_{id} as shown in equation 2.3.

$$W_{1d} = E_1 \omega \eta_{1d} \quad (2.3)$$

where E_1 is the energy of the first subsystem and ω being the angular frequency. The power flow between subsystems are determined by coupling loss factors (CLF), η_{ij} . The definition of the coupling loss factors are similar to that of the internal loss factor and is shown in equation 2.4.

$$W_{12} = E_1 \omega \eta_{12} \quad (2.4)$$

By using these definitions of CLFs and internal loss factors equation 2.1 and 2.2 can be rewritten as equation 2.5 and 2.6.

$$W_1 + E_2 \omega \eta_{21} = E_1 \omega (\eta_{1d} + \eta_{12} + \eta_{13}) \quad (2.5)$$

$$W_2 + E_1 \omega \eta_{12} = E_2 \omega (\eta_{2d} + \eta_{21} + \eta_{23}) \quad (2.6)$$

From these sets of power balance equations it is possible to calculate the energies of each subsystem by finding expressions for the coupling and internal loss factors. [2]

In SEA it is assumed that the transmission of energy between the subsystems is proportional to the difference in modal energy [3]. The modal energy can be expressed as in equation 2.7

$$E_{modal} = \frac{E}{n \Delta \omega} \quad (2.7)$$

with E being the energy in the subsystem, n being the modal density in the system and $\Delta \omega$ being a mean value taken over a frequency band including a number of modes around the angular frequency ω . Combining this with the above assumption the net power between two subsystems can be written as show in equation 2.8

$$net \ power \ flow = W_{12} - W_{21} = b \left(\frac{E_1}{n_1 \Delta \omega} - \frac{E_2}{n_2 \Delta \omega} \right) = b' \left(\frac{E_1}{n_1} - \frac{E_2}{n_2} \right) \quad (2.8)$$

with b and $b' = \frac{b}{\Delta \omega}$ being proportionality factors. Combining this with the definition for the CFLs in equation 2.4 gives

$$\frac{b'}{n_1} = \omega \eta_{12} \quad (2.9)$$

$$\frac{b'}{n_2} = \omega \eta_{21} \quad (2.10)$$

and from there the following expressing can be shown

$$n_1 \eta_{12} = n_2 \eta_{21} \quad (2.11)$$

The equation shown in 2.11 is called the reciprocity or consistency relation. This expression can be useful for determining CLFs if one of the CLFs are known and the modal density of the subsystems are known.

2.1.1 Modes

One of the foundations of SEA theory are the assumption that the response of a subsystem is determined by resonant modes. To make an accurate statistical prediction of the responses between the modes of a subsystem the number of modes must be high. If this is not the case the prediction of the coupling and response between these modes may include errors. The number of modes per frequency band that is sufficient to make accurate predictions is suggested to be between 2 and 30 depending on the literature [4]. It is important to note that this is not an absolute and the accuracy of the model may decline gradually. Another important parameter to determine the accuracy of a SEA model is the modal overlap of a subsystem. Modal overlap is defined as "the ratio of the modal bandwidth to the average frequency spacing between modes" [4] and is calculated as

$$M = f\eta n \quad (2.12)$$

with η being the total loss factor of the subsystem and n being the modal density. Higher modal overlap will give a more uniform frequency response. The modal overlap is important as it takes into account not only the modes of modes but also the damping of these modes. With a large number of modes the frequency spacing of these mode becomes smaller. This leads to an increase in the modal overlap. High damping gives wider resonance peaks and makes the bandwidth larger.[5]. It is preferable if the modal overlap is more than 1. An assumption in SEA theory states that a subsystem should be damping controlled [4].

In the SEAWOOD software the modal density of an orthotropic subsystem is derived from the dynamical equations describing the subsystem as briefly discussed in section 2.5.5. From the modal density the number of modes in the frequency band of interest is calculated as

$$N(\omega\Delta\omega) = \int_{\Delta\omega} n(\omega)d(\omega) \quad (2.13)$$

with n being the modal density.

For a homogeneous three dimensional room the modal density is calculated as

$$n(\omega) = \frac{\omega^2 V}{2\pi c^3} + \frac{\omega A}{8\pi c^2} + \frac{P}{16 c} \quad (2.14)$$

with V being the volume of the room, A the total area of the room and P the perimeter of the room. [6]

For the simplified model the number of modes in each frequency band and also the modal overlap was important to calculate. The modal density of the CLT140 plate was calculated for bending waves on a homogeneous thin plate as

$$n(f) = \frac{\pi S f c_{eff}}{c^2} \quad (2.15)$$

with S being the surface of the plate, $f c_{eff}$ being the effective critical frequency and c being the speed of sound in air. The equation above is valid for plates with simply supported edges. According to literature

most walls and floors can be seen as simply supported panels with only a small amount of clamping [4]. From the modal density the number of modes in each frequency band can be calculated as

$$N = n(f)\Delta f \quad (2.16)$$

with Δf being the bandwidth of the band. In this case third octave bands are used so Δf is 0.23 times the centre frequency of the band.

2.2 CLFs

2.2.1 CLFs for structure-cavity interaction

To determine the CLFs for the interaction between a room and a wall, the radiation efficiency σ can be used. σ is defined as

$$\sigma = \frac{W_{rad}}{W_{plane}} = \frac{W_{rad}}{\bar{v}\rho_0 S} \quad (2.17)$$

with W_{rad} being the radiated power, \bar{v} the rms value of the average vibrations velocity, S the surface of the radiating object. W_{plane} is the radiated power of flat surface generating a plane wave and is used in the definition in relation with the radiated power of the object. By using that the radiating energy is the energy that is flows out of subsystem 1 and using the definition for CLFs from equation 2.4 the following expression is attained.

$$W_{rad} = W_{12} = E_1 \omega \eta_{12} \quad (2.18)$$

This can be rewritten to find the CLF as

$$\eta_{12} = \frac{\bar{v}\rho_0 S \sigma}{\omega E_1} \quad (2.19)$$

By using that $E_1 = m'' S \bar{v}$ equation 2.19 can be written as the general CLF for wall to air as seen in equation 2.20

$$\eta_{plate-air} = \frac{\rho_0 c \sigma}{2\pi f m''} \quad (2.20)$$

with m'' being the mass per unit area.

2.2.2 CLFs for cavity-structure interaction

To find the air to wall CLF the reciprocity relation from equation 2.11 can be used. To use the reciprocity relation the modal density of the room and the plate and the CLF η_{12} needs to be found. By calling the air subsystem 2 and calling the plate subsystem 1, equation 2.20 can be used for η_{12} . The modal density of an air volume is defined as

$$n_2 = \frac{L_2}{c} + \frac{\pi f S_2}{2c^2} + \frac{4\pi f^2 V_2}{c^3} \quad (2.21)$$

with L_2 being the total length of the edges of the room and S_2 being the total surface of the room. The last term of the equation dominates the expression for higher frequencies. For calculating the CLF in this case only the last term will be used for this reason. The modal density for a plate with bending waves can be expressed as

$$n_1 = \frac{S_1}{2} \sqrt{\frac{m''}{B}} = \frac{\pi S_1 f_c}{c^2} \quad (2.22)$$

with B being the bending stiffness, f_c being the critical frequency and c being the speed of sound in air. By using the reciprocity relation the CLF for air to plate can be expressed as

$$\eta_{air-plate} = \eta_{21} = \eta_{12} \frac{n_1}{n_2} = \frac{\rho_0 c \sigma S_1 f_c}{8\pi f^3 m'' V_2} \quad (2.23)$$

2.2.3 CLFs for structure-structure interaction

See section 2.5.3

2.2.4 CLFs for direct transmission

Energy transfer between two subsystems can happen through non-resonant transmission also commonly called direct transmission or mass law. For example a SEA model with a wall separating two rooms with the wall not seen as a resonant system and cannot be modelled as a SEA subsystem. The CLF for such a case when there is energy transmission from room to room can be described as follows. The definition of transmission coefficient τ is

$$W_t = W_i \tau \quad (2.24)$$

with W_i being the incident power on the surface and W_t being the transmitted power. For a diffuse field in 3-D the incident power may be expressed as

$$W_i = \frac{EcS}{4V} \quad (2.25)$$

with S being the surface of the dividing partition between the rooms and V being the volume of the sending room. Using the definition of the CLF found in equation 2.4 the following CLF for direct transmission can be found

$$\eta_{room-room} = \frac{cS}{8\pi fV} \tau_{room-room} \quad (2.26)$$

The transmission coefficient for the direct transmission can be found from the reduction index R and that

$$\tau = 10^{-R/10} \quad (2.27)$$

2.3 Damping

The energy that leaves the subsystems are generally referred to as damping. If the energy loss in the subsystem is due to power transfer between two coupled systems the CLFs described earlier is used. All other forms of losses in the subsystem are called internal loss factors and are described as in equation 2.3. The internal losses usually consist of vibrational energy that converts into heat. The internal loss factor also consist of the losses that occurs due to coupling between elements not induced in the SEA model. [4]. The total damping of the system is called the total loss factor and is the sum of the internal and coupling loss factors. The total loss factor for i subsystems is given by

$$\eta_i = \sum_{i=1, j \neq i}^n \eta_{ij} + \eta_{id} \quad (2.28)$$

Reverberation time is commonly used in building acoustics to measure damping in a system. However it may be hard to measure the reverberation time for a structure due to the short reverberation time. It may also be hard to excite a building structure with steady noise. The relation between the reverberation time and the total loss factor can be described as

$$\eta_i = \frac{\ln(10^6)}{2\pi fT} = \frac{2.2}{fT} \quad (2.29)$$

with T being the time it takes for the energy to decay with 60 dB from the end of the excitation source. The reverberation time can be estimated from Sabine's equation as

$$T = \frac{0.161V}{A} = \frac{0.161V}{\sum S\alpha} \quad (2.30)$$

with A being the total absorption area of the room calculated as the sum of the product of the surface area and their corresponding absorption coefficients, and V being the volume of the room. The total loss factor can then be described as

$$\eta_i = \frac{13.7 \sum S\alpha}{fV} \quad (2.31)$$

If the absorption area or reverberation time are unknown a standard approximation may be used. The absorption area is then assumed to be 10 m² and the reverberation time 0.5 s. [4]

Some internal loss factors can be estimated by certain expressions. Equation 2.32 by Craik are used to estimate the internal loss factor for concrete plates used in some of the calculated layups. [3]

$$\eta_{int} = \frac{1}{\sqrt{f}} + 0.015 \quad (2.32)$$

2.4 Solving the power balance equations

When all the coupling and total loss factors have been determined for each subsystem the power balance equations can be solved for the energy levels in each subsystem as

$$\omega \begin{bmatrix} \eta_i & -\eta_{ji} & \cdots & -\eta_{k1} \\ -\eta_{ij} & \eta_j & \cdots & \\ \vdots & \vdots & \ddots & \vdots \\ -\eta_{ik} & \cdots & \cdots & \eta_k \end{bmatrix} \begin{bmatrix} E_i \\ E_j \\ \vdots \\ E_k \end{bmatrix} = \begin{bmatrix} W_i \\ W_j \\ \vdots \\ W_k \end{bmatrix}$$

for k subsystems, with n_i being the total loss factor shown in equation 2.28 and η_{ij} being the CLF between subsystems i and j . The energies in the subsystem can then be used to calculate the spatial average sound pressure $\langle p^2 \rangle$ in an acoustic cavity by the relation

$$E = \frac{\langle p^2 \rangle V}{\rho c^2} \quad (2.33)$$

With V being the volume of the cavity, ρ being the density of the fluid in the cavity and c being the wave speed in the medium.

2.5 SEAWOOD Theory

2.5.1 CLFs structure-cavity and cavity-structure

SEAWOOD calculates these CLFs as described in sections 2.2.1 and 2.2.2.

2.5.2 CLFs Direct transmission

CLFs for the direct path between two cavities are calculated as shown in equation 2.26. The transmission between the two rooms are described as non resonant transmission or the so called mass law. The diffuse field transmissions coefficient τ_d used to calculate mass law transmission can be calculated as

$$\tau_d = 2 \int_0^{\pi/2} \tau(\theta) \sin\theta \cos\theta d\theta \quad (2.34)$$

with θ begin the angle of incidence. The transmission coefficient for a certain incident angle $\tau(\theta)$ are found by using the transfer matrix method and using a correction based on spatial windowing [6]. As the transfer matrix method assumes that the mass partition is infinite in size a spatial windowing is used to estimate a finite sized mass partition. The finite transmission coefficient τ_F is estimated from a plane wave passing through a rectangular diaphragm of a certain length and width. If the media on both sides of the partition is the same τ_F can be written as a function of the transmission coefficient for an infinite case τ_∞ as

$$\tau_F = \tau_\infty \sigma_{rad} \cos(\theta) \quad (2.35)$$

The infinite transmission coefficient attained from the transfer matrix method are multiplied by the radiation factor of the diaphragm and the cosine of the incidence angle. The finite transmissions coefficient can then be used to calculate the diffuse filed transmission coefficient used for calculation the CLF for direct transmission between rooms.

2.5.3 CLFs for structure-structure interaction

In SEAWOOD the coupling loss factor used for structure to structure interaction are calculated from wave theory. For a semi-infinite media that is coupled by a infinite length junction the wave propagation is solved and used to find out the CLFs. An assumption that both the sending and receiving parts are diffuse are made. The waves carrying energy through the junction between two subsystems are attenuated depending on the boundary conditions and the material characteristics of the coupled media. Using the expression for the diffuse field transmission coefficient found in equation 2.34 the integral for a 2D case i.e a thin plate, can be shown by assuming diffuse field pressure \tilde{p} as

$$\frac{\tilde{p}}{p_0 c} l \int_{-\pi/2}^{\pi/2} \cos\theta \frac{d\theta}{2\pi} = \frac{\tilde{p}}{p_0 c} \frac{l}{\pi} \left(= \frac{\epsilon_D c l}{\pi} \right) \quad (2.36)$$

the transmissions coefficient is then defined as

$$W_{through} = W_{inc} \tau \quad (2.37)$$

by using the described properties of a 2D diffuse field the incident power can be described as

$$W_{inc} = I_D l = \frac{E c_{g1} l}{\pi i S} \quad (2.38)$$

with I_D being the diffuse intensity, c_{g1} the group speed in the first plate subsystem, l being the length of the junction and S being the surface of the sending plate. By using the definition for the coupling loss

factor $W_{through} = E_1 \omega \eta_{12}$ the expression for the coupling loss factor between two plates can be described as [2]

$$\eta_{12} = \frac{c_g l}{2\pi^2 f S} \tau_{12} \quad (2.39)$$

For all the structure to structure connection used in the model a line connection is used as described above. Point connections are used to model certain elements. The point connection uses the driving point impedance on the junction edge to calculate the power flow between the subsystems. The point junction coupling loss factor are calculated in the software as

$$\eta_{12} = \frac{1}{2\pi\omega} \frac{\tau_{12}}{n(\omega)} \quad (2.40)$$

with $n(\omega)$ being the modal density of the wave field supporting the propagation in the emitter subsystem [7].

2.5.4 Trim

A trim layer is used in SEAWOOD to model different types of sound insulation layers that cannot be modelled as subsystems. The calculations of these trim layers are done in an module of SEAWOOD called SEA-Foam. From these calculations the module provides the insertion or transmission loss for the trim layer. To make these predictions, SEA-Foam uses the Transfer matrix method. This method are more closely explained in various literature [5] [3] [8] and will only briefly be discussed here. The trim layer is divided into sub layers and an matrix for each layer is created to derive the pressure and velocity for each side of the layer. The matrices are then assembled to provide a relationship between the pressure and velocity for each side of the whole trim layer [6] [8].

2.5.5 Orthotropic Modal Thin Plate

The flat plate subsystem are used in SEAWOOD to model for example a wall or a floor. The plate subsystem is orthotropic and supports flexural, extension and shear wave-types. For high frequencies the energies in the subsystem consists of both flexural and in-plane energies.

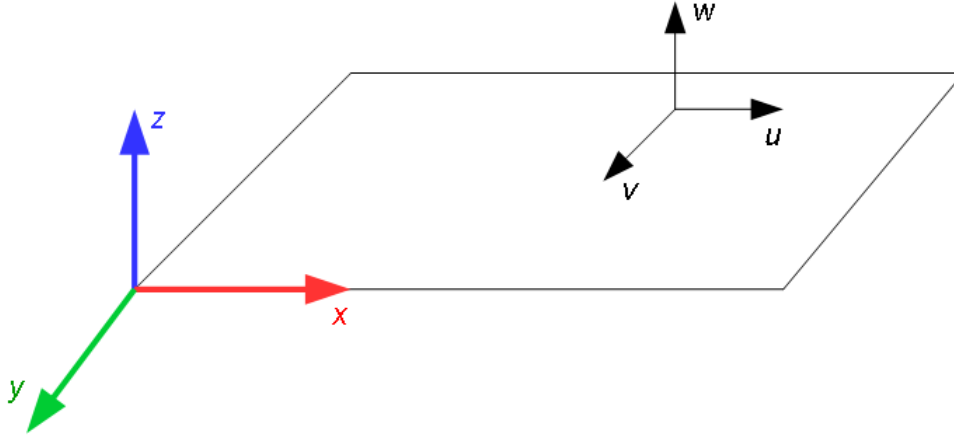


Figure 2.2: Model of the orthotropic plate with x being the length of the plate and y width

The following three equations describe the relations between the wave amplitudes v, u, w and the inertial forces of the plate. The behaviour of a orthotropic thin plate is described by the elastic coefficients C_{ij} and bending stiffness D_{ij} which makes up the stiffness matrix. The coefficients are material dependent and are described as

$$\begin{aligned}
 C_{11} &= \frac{E_x h}{1 - \nu_x \nu_y}, C_{66} = Gh, C_{12} = \frac{\nu_x E_y h}{1 - \nu_x \nu_y}, C_{22} = \frac{E_y h}{1 - \nu_x \nu_y} \\
 D_{11} &= \frac{E_x h^3}{12(1 - \nu_x \nu_y)}, D_{66} = \frac{Gh^3}{12}, D_{12} = \frac{\nu_x E_y h^3}{12(1 - \nu_x \nu_y)}, D_{22} = \frac{E_y h^3}{12(1 - \nu_x \nu_y)}
 \end{aligned} \tag{2.41}$$

E_x, E_y Young's moduli in x and y directions
 G shear modulus
 with h thickness of the plate
 ν_x, ν_y Poisson's coefficients in x and y directions
 ρ mass density of the plate material

C_{ij} and D_{ij} can be related to the shell displacement through differential equations as

$$\begin{aligned}
 C_{11} \frac{\partial^2 u}{\partial x^2} + C_{66} \frac{\partial^2 u}{\partial y^2} + (C_{12} + C_{66}) \frac{\partial^2 v}{\partial x \partial y} &= \rho h \frac{\partial^2 u}{\partial t^2} \\
 C_{22} \frac{\partial^2 v}{\partial y^2} + C_{66} \frac{\partial^2 v}{\partial x^2} + (C_{12} + C_{66}) \frac{\partial^2 u}{\partial x \partial y} &= \rho h \frac{\partial^2 v}{\partial t^2} \\
 D_{11} \frac{\partial^4 w}{\partial x^4} + D_{22} \frac{\partial^4 w}{\partial y^4} + 2(D_{12} + 2D_{66}) \frac{\partial^4 w}{\partial x^2 \partial y^2} &= -\rho h \frac{\partial^2 w}{\partial t^2}
 \end{aligned} \tag{2.42}$$

For a simply-supported plate the displacement field is expressed as

$$\begin{aligned}
 u &= U_{nm} \sin(k_n y) \sin(k_m x) e^{-i\omega t} \\
 v &= V_{nm} \sin(k_n y) \sin(k_m x) e^{-i\omega t} \\
 w &= W_{nm} \sin(k_n^f y) \sin(k_m^f x) e^{-i\omega t}
 \end{aligned} \tag{2.43}$$

From the calculation of the eigenvalues for equation 2.42 the eigenwavenumbers for the plate can be found. w is not coupled to u and v and therefore the wavenumbers for the in plane waves are given by k_{mn} and the wavenumbers for flexural waves are given by k_{nm}^f . These wavenumber are then used to find the statistical wavenumber for use in calculating CLF's. All discrete k_{nm} for each eigenvalue of the dynamical subsystem are averaged in a frequency band as

$$\langle k \rangle = \langle k(\omega_c, \Delta\omega) \rangle_{mn} = \langle \sqrt{k_m^2 + k_n^2} \rangle_{\omega_{mn} \pm \Delta\omega} \tag{2.44}$$

Below the first mode the wavenumber is set equal to that of the first mode. If the mode count in a band is zero the wavenumber is interpolated. $\langle k \rangle$ is called the mean interpolated wavenumber. Another wavenumber called the statistical wavenumber is computed from the band-averaged discrete modal density n_d as

$$k_s = k_s(\omega_c, \Delta\omega) = \sqrt{\frac{2\omega_c n_d}{S}} \tag{2.45}$$

In frequency bands where mode count is zero the statistical wavenumber is coerced to the obtained values for the mean interpolated wavenumber. This lead to one final wavenumber called the mean statistical wavenumber $\langle k_s \rangle$. [6]

2.5.6 Radiation efficiency

To calculate the CLF for a structure to cavity case, equation 2.20 is used. To calculate the radiation efficiency used to find the CLF, SEAWOOD uses spatial windowing for finite plates as described by [9]. By assuming a diffuse vibration field on a flat structure as a sum of freely propagating waves, each having the wavenumber $k_s(\omega)$ the structural averaged radiation efficiency $\overline{\sigma}_d(\omega)$ can be expressed as

$$\begin{aligned}
 \overline{\sigma}_d(\omega) &= \frac{S}{2\pi^3} \int_0^{2\pi} \int_0^{k_a} \int_0^{2\pi} \frac{1 - \cos((k_r \cos\phi - k_s \cos\psi)L_x)}{[(k_r \cos\phi - k_s \cos\psi)L_x]^2} \frac{1 - \cos((k_r \sin\phi - k_s \cos\psi)L_y)}{[(k_r \sin\phi - k_s \cos\psi)L_y]^2} \\
 &\quad \frac{k_a k_r}{\sqrt{k_a^2 - k_r^2}} d\phi dk_r d\psi
 \end{aligned} \tag{2.46}$$

with the wavenumber in air $k_a = \frac{\omega}{c}$ and L_x and L_y being dimensions of the plate. [6]

2.5.7 Uniform section, static and dynamic laminates

For modelling the CLT plates three different methods are used. The simplest way was to model the CLT plate as a solid plate called uniform section. In reality the CLT plates are made up of laminated timber. In SEAWOOD this can be represented by either a static or dynamic laminate. The static laminate section is considered an orthotropic section where each layer contributes its static inertia to calculate the material properties for the whole section. For the dynamic laminate the different layers are cross coupled to each other. Depending on the material properties involved the layers becomes uncoupled with the increase in frequency [10].

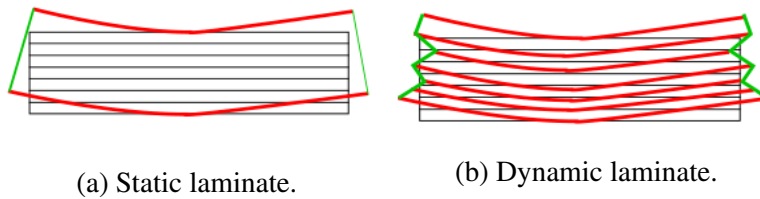


Figure 2.3: Figures from [10]

2.6 Simplified SEA model

In order to validate the calculations made by the SEAWOOD software a simplified SEA model was made. The model tries to predict the sound reduction index between a plate made of CLT. Three subsystems were used for the model as seen in figure 2.4. With subsystem 1 and 2 being the sending and receiving room and subsystem 3 being the wood plate.

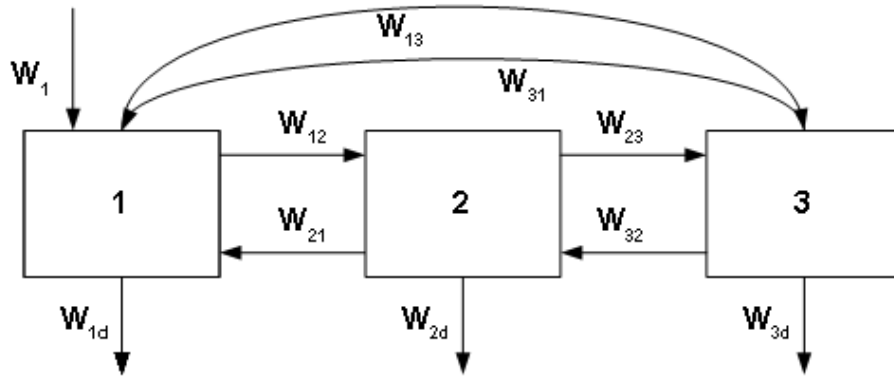


Figure 2.4: SEA model of a CLT plate separating two rooms.

Using the calculations for the CLFs described in section 2.2 , the following power balance matrix can be set up to calculate the energies in each subsystem.

$$\omega \begin{bmatrix} \eta_1 & -\eta_{21} & -\eta_{31} \\ -\eta_{12} & \eta_2 & -\eta_{32} \\ -\eta_{13} & -\eta_{23} & \eta_3 \end{bmatrix} \begin{bmatrix} E_1 \\ E_2 \\ E_3 \end{bmatrix} = \begin{bmatrix} W_1 \\ 0 \\ 0 \end{bmatrix}$$

The calculation for the CLF concerning structure to air and vice versa uses the radiation efficiency σ . For these calculation σ is approximated to be 1 for all frequencies. The transmission coefficient used to calculate the CLF for direct transmission between the rooms were calculated by using equation 2.27 with R being the reduction index of the CLT plate approximated for a diffuse field for $f < f_c$ as

$$R = 20 \log(f m'') - 42.5 \quad (2.47)$$

with m'' being the mass per unit area calculated as $m'' = \rho h$. As the CLT plates are considered orthotropic an effective bending stiffness are used to calculated an effective critical frequency [11]. The effective critical frequency $f_{c_{eff}}$ is calculated as

$$f_{c_{eff}} = \frac{c^2}{2\pi} \sqrt{\frac{m''}{B_{eff}}} \quad (2.48)$$

with c being the speed of sound in air and the effective bending stiffness B_{eff} calculated as

$$B_{eff} = \sqrt{B_{strong} B_{weak}} \quad (2.49)$$

with the bending stiffness in the weak direction of the wood calculated as

$$B_{weak} = \left(\frac{E_{weak} h^3}{12(1 - \nu)} \right) \quad (2.50)$$

and the bending stiffness of the strong direction calculated as

$$B_{strong} = \left(\frac{E_{strong} h^3}{12(1 - \nu)} \right) \quad (2.51)$$

As the CLT plate used in the model is 140 mm thick it may not be considered thin as the plate theory assumes. An approximation of the frequency limit for bending waves on thin plates can be calculated as

$$f_{B(thin)} \approx \frac{0.05 c_{L,peff}}{h} \quad (2.52)$$

with $c_{L,peff}$ being the effective quasi longitudinal phase velocity in plates and h being the thickness of the plate.

The effective quasi longitudinal phase velocity can be calculated as

$$c_{L,peff} = \frac{B_{eff} 12}{h^3 \rho} \quad (2.53)$$

Thin plate theory can extend up to four times above the frequency limit. For a solid homogeneous plate, the error range between the limit and four times the limit is usually less than 3 dB [11]. To evaluate the accuracy of the SEA model the first resonance frequency of the plate using an effective critical frequency is calculated as

$$f_{11} = \frac{c^2}{f_c} \frac{1}{L_x^2} + \frac{1}{L_y^2} \quad (2.54)$$

with L_x and L_y being the length of the sides of the plates.

The above equation are valid for a thin homogeneous, simply supported plate. The equation is used when calculating the first resonance frequency for concrete and gypsum plates used in the layups. For the orthotropic CLT plates the following expression is used to calculate the first resonance frequency.

$$f_{i,n} = \frac{\pi}{2\sqrt{m}} \left[\frac{i^4}{a^4} B_x + \frac{n^4}{b^4} B_y + \frac{2i^2 n^2}{a^2 b^2} B_{xy} \right] \quad (2.55)$$

with m being the mass per unit area, a and b being the length and width of the plate and i, n defining a mode of vibration. As neither of these indices can be zero the first resonance frequency of the plate is

found at f_{11} . The bending stiffness of the directions are calculated as

$$B_x = \frac{E_x h^3}{12(1 - \nu_{xy}\nu_{yz})} \quad (2.56)$$

$$B_y = \frac{E_y h^3}{12(1 - \nu_{xy}\nu_{yz})} \quad (2.57)$$

$$B_{xy} = B_x \nu_{yz} + 2 \frac{G_{xy} h^3}{12} \quad (2.58)$$

with ν being Poisson's ratio in the different directions, h being the thickness of the plate and G being Shear's modulus. The internal loss factor η_{int} are approximated as 0.01. The approximation for the total loss factor of the plate is only valid for $m'' < 850 \text{ kg}^2$ and calculated as

$$\eta_{tot,lab} = \eta_{int} + \frac{m''}{485\sqrt{f}} \quad (2.59)$$

Using the relation between energy and the spatial average sound pressure described in equation 2.33 the sound pressure level for the rooms can be calculated as

$$Lp_{room} = 10 \log \left(\frac{P_{room}}{2e-5} \right) \quad (2.60)$$

The standard method for calculating sound reduction index is the used to calculate the reduction index of the CLT plate.

$$R = Lp_{sending} - Lp_{receiving} + 10 \log \left(\frac{S_{plate}}{A} \right) \quad (2.61)$$

with S_{plate} being the surface area of the plate and A being the total absorption area of the receiving room calculated as

$$A = \frac{0.161V}{T} \quad (2.62)$$

with V being the volume of the receiving room and T the reverberation time as described in section 2.3 The radiation efficiency of of the CLT plate are calculated as described in standard EN 12354-1 using the effective critical frequency.

3 SEAWOOD software

The SEAWOOD software is based on a previous existing software called SEA+. There are numerous settings and tweaks that can be made and thus they will not all be explained here. If not stated otherwise the default settings are always used when simulating the models. What is described here is the general layout of the workspace and how the different subsystems and connections are represented in the software. Figure 3.1 shows the workspace and a model with different subsystems and connection.

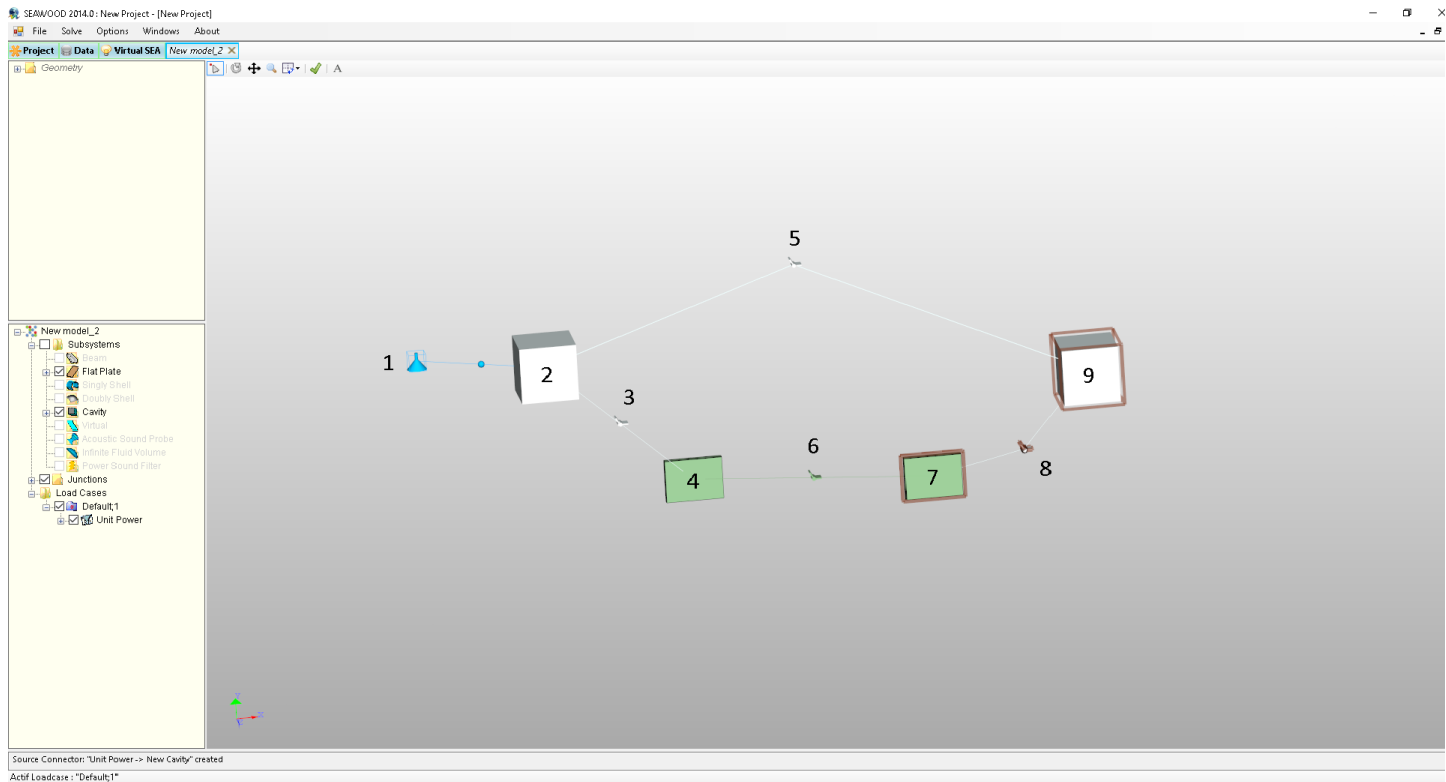


Figure 3.1: Workspace of the SEAWOOD software.

1. This is the source that inputs energy into the chosen subsystem and it is set to 1W.
2. The white cube is the subsystem used when modelling rooms and cavities.
3. This white line represents the connection between a cavity and a plate subsystem
4. The green rectangle is used for plate subsystems
5. The connection between two room subsystem representing direct transmission looks the same as the line between a cavity subsystem and a plate subsystem.
6. A green line are used to model a connection between two plate subsystems.
7. The green plate subsystem with a red frame are used to model a plate with an added trim layer.
8. A white line with a red middle part are used to add the insertion loss of the trim layer element to the path between a plate subsystem and a cavity subsystem.
9. The white cube with a red frame are used to represent a cavity/room with an added trim layer.

4 Estimating input data using parameter variation

One of the challenges in this project was how the CLT plate could be modelled in the software in aspect to the behaviour of the wood. It is challenging to determine the material parameters for these type of wooden plates due to differences between different wood types. It is also difficult to properly determine the parameters of wood due to the material being different depending of how the tree has grown. A parameter study of the material was conducted in the SEAWOOD software to find out the optimal properties to use in the software validation. The material study was conducted by starting with the material properties found in literature and then changing the values of the properties. The starting properties were taken from [12] and [13]. These material properties are attained from a three-layer CLT plate made of spruce and having strength class C24. The CLT plates used in the constructions in this thesis are between 100 and 320 millimeter thick and with the exception of the thickest, the plates are made up of five layers. The thickest plate are made of eight layers. This will probably affect the parameters of the wood. A measurement of a single CLT plate, 140 millimeter thick with strength class C24 and made of spruce [14] are available. As this plate have reliable measurements this plate will be used as a base for determine the material parameters to be used. To find out the best parameter to use in the model the measured reduction index between two rooms with the CLT plate in between was compared with the modelled reduction index. All data in the figures are presented in third octave bands.

Figure 4.1 shows a comparison of material density. The values are based of a study of a three layer CLT plates made out of black spruce. Depending on the quality class of the wood the density is between 433 and 605 kg/m³ [15]. Hopkins lists soft wood at a density of 440 kg/m³ [11]. The density part of the parameter study will therefore start at 430 kg/m³ and then increase with steps of 20 to find out how the different density changes the resulting reduction index. The arbitrary increase in density is to try to cover the parameter range mentioned in literature.

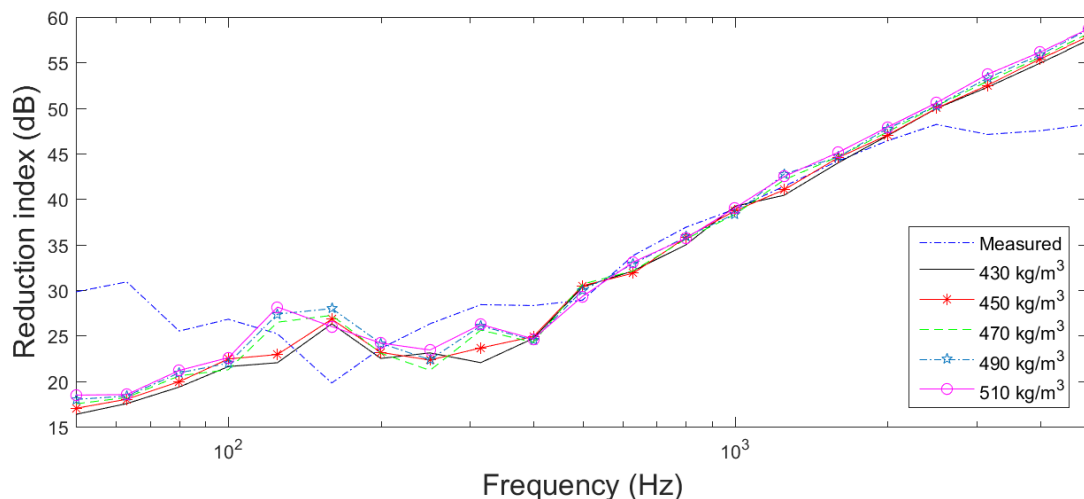


Figure 4.1: Reduction index of a CLT140 plate separating two rooms with different values for density of the material.

From the density comparison in figure 4.1 shows that the biggest difference between the different

densities of the material mostly affect the areas of around the critical frequencies of the material between about 100 to 500 Hz.

	<i>Measured</i>	430 (kg/m ³)	450 (kg/m ³)	470 (kg/m ³)	490 (kg/m ³)	510 (kg/m ³)
R_w	36 dB	34 dB	34 dB	34 dB	35 dB	35 dB

Table 4.1: Resulting weighted reduction index from the sound level measurement compared to the resulting index from the density change in the material

Table 4.1 shows that the higher densities gives a better weighted reduction index. The curves of the calculated values for densities 490 and 510 kg/m³ are closest to the measured results. The density of 490 kg/m³ are chosen for as the modelling parameter because it is closer to both the starting values from the literature as well as the average values from [15]. It should be noted that at higher frequencies (here about 2500 Hz) the measured curves sometimes start to form a plateau. This appearance, which may be due to the physical behaviour of the CLT, is discussed further in Chapter 6.

To investigate how shears modulus affects affects the simulation, the model was first made with the data taken from the literature described earlier. The value of shears modulus was then increased to 20 percent of the original value and also decreased the same amount. Shears modulus was also calculated as for an isotropic plate. Figure 4.2 shows resulting reduction index curves for the different parameter values and table 4.2 shows the resulting calculated weighted reduction index. The biggest difference are located around 100 to 500 Hz. The calculated isotropic value gives the best weighted reduction index but is also a lot higher then the other values. Despite the large difference from the literature data the isotropic value was chosen as a parameter for shears modulus due to better coinciding with the measurement.

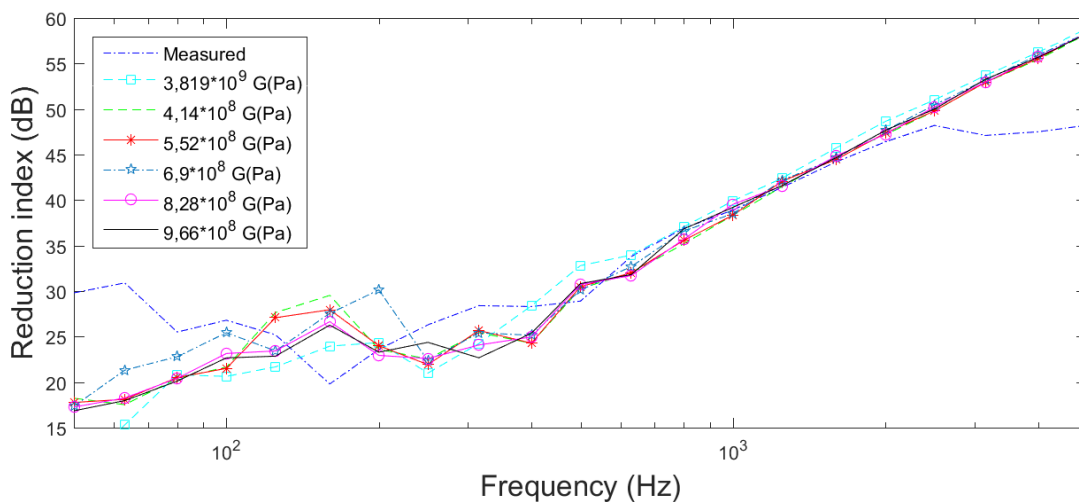


Figure 4.2: Reduction index of a CLT140 plate separating two rooms with different values for shears modulus of the material.

	Measured	Isotropic	-40%	-20%	Literature	+20%	+40%
$G(Pa)$	-	$3,819e9$	$4,14e8$	$5,52e8$	$6,9e8$	$8,28e8$	$9,66e8$
R_w	36 dB	36 dB	34 dB	34 dB	35 dB	34 dB	35 dB

Table 4.2: Resulting weighted reduction index from the measurement compared to the resulting index from the change in shears modulus of the material

Young's modulus for the orthogonal directions x and y was investigated in the same way as described above. Figure 4.3 shows the resulting reduction index for the different simulations with different values for Young's modulus for the stiffest direction of the wood. In this case this is labelled as direction x. Again the largest differences between the parameters are in the frequency range of 100-500 Hz. Table 4.3 shows the weighted reduction index calculated from the curves. The parameter value that is 20 and 40 percent more than the literature suggest are the ones that seems to coincide the best with the measured reduction index. The values that is 20 percent more than the literature was chosen as a modelling value due to being closer to the parameter value from the literature.

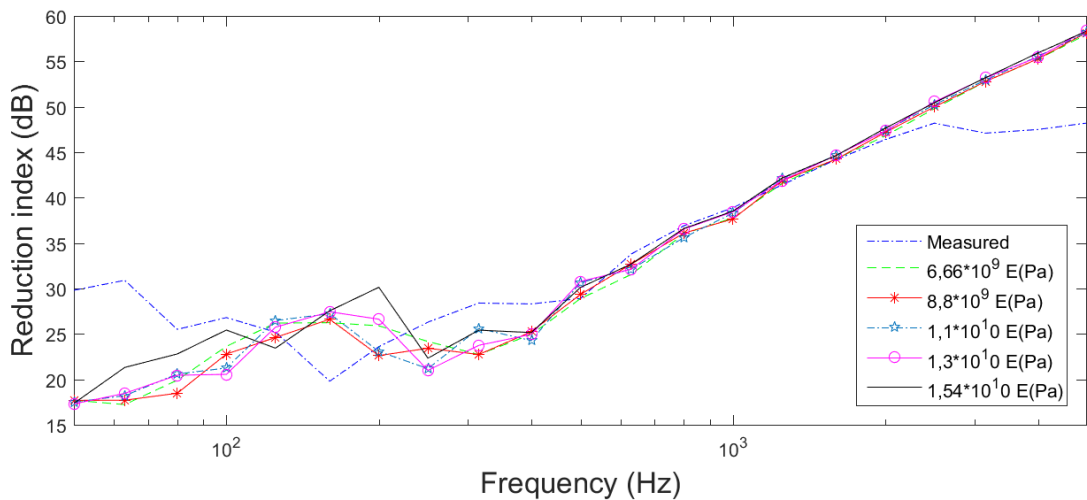


Figure 4.3: Reduction index of a CLT140 plate separating two rooms with different values for Young's modulus in the x direction of the material.

	Measured	-40%	-20%	Literature	+20%	+40%
$E_x(Pa)$	-	$6,66e9$	$8,8e9$	$1,1e10$	$1,3e10$	$1,54e10$
R_w	36 dB	34 dB	34 dB	34 dB	35 dB	35 dB

Table 4.3: Resulting weighted reduction index from the sound level measurement compared to the resulting index from the change in Young's modulus in the x direction of the material the material

For the Young's modulus of the y direction the same procedure as described above was applied. Figure 4.4 shows the resulting reduction index curves for the different parameters of the wood. As with the other graphs the largest difference is found in the 100-500 Hz region. Table 4.4 shows the resulting weighted reduction index calculated from the curves. Both the lower parameter value and the one that was raised 20 percent over the original value have the same weighted reduction index. However the curve from the simulation with parameter value $2,96 * 10^8 \text{ Pa}$ i.e the 20 percent reduction of the value corresponds better the measured reduction index in the the 500-1500 Hz region. An that is way that value is chosen for future simulations.

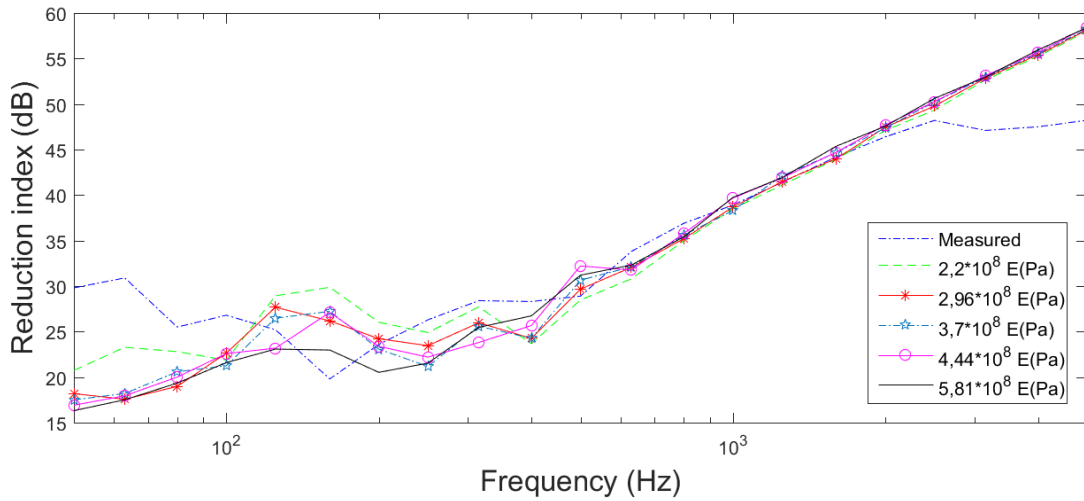


Figure 4.4: Reduction index of a CLT140 plate separating two rooms with different values for Young's modulus in the y direction of the material.

	Measured	-40%	-20%	Literature	+20%	+40%
$E_y(\text{Pa})$	-	$2,2e8$	$2,96e9$	$3,7e8$	$4,44e8$	$5,81e8$
R_w	36 dB	35 dB	35 dB	34 dB	35 dB	34 dB

Table 4.4: Resulting weighted reduction index from the sound level measurement compared to the resulting index from the change in Young's modulus in the y direction of the material the material

Table 5.18 shows the parameter values from the literature and the resulting values from the investigation.

	E_x (Pa)	E_y (Pa)	G_{xy} (Pa)	ρ (kg/m ³)	ν_{xy}	ν_{yz}
Literature	$1,1e10$	$3,7e8$	$6,9e8$	470	0.44	0.64
Trimed	$1,54e10$	$2,96e8$	$3,819e9$	490	0.44	0.64

Table 4.5: Parameter values from literature [12] [13] and the trimmed values from the investigation with Young's modulus in x and y direction, E_x and E_y . Shears modulus G_{xy} , the internal loss factor of the plate, η_{im} , the material damping $\eta_{damping}$, the density ρ and Poisson's ratio for directions ν_{xy} and ν_{yz}

The chosen material parameters was used in the modelling and an investigation regarding the internal loss factor of the CLT plate was conducted. Figure 4.5 shows the tested internal loss factors in steps of 0.005 for all frequency bands. The figure shows that increasing the internal loss factor gives a higher reduction index.

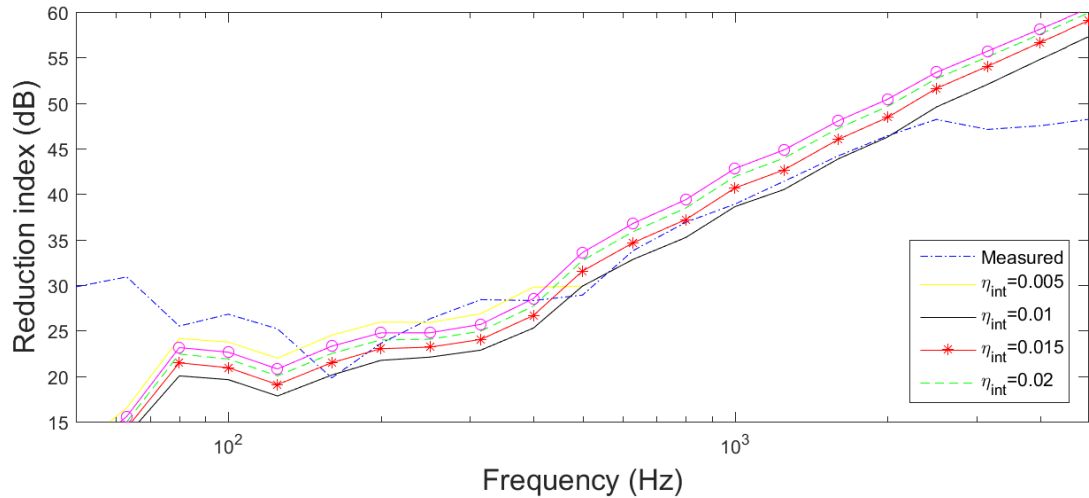


Figure 4.5: Comparison between different internal loss factors of the uniform CLT140 plate.

To get the best coincidence with the measured results the internal loss factor was made frequency dependent. These values are found in table 4.6

Using the data obtained from the parameter study a comparison was made between the parameters from the literature and the ones from the study. Figure 4.6 shows this comparison. There is not a very large difference between the literature curve and the trimmed curve. However, for almost all of the 1/3-octave bands the trimmed curve coincide with the measured curve better then the literature one. The weighted reduction index is 36 dB for the trimmed curve and 35 for the literature. There is also another curve displayed in the graph. The plate was modelled as an isotropic plate with the same parameters as the others. The literature [12] [13] indicates that the CLT plate is highly orthotropic and this can clearly be seen in the figure with the isotropic curve fitting poorly with the measurement.

Frequency (Hz)	η_{int}
50	0,03
63	0,03
80	0,03
100	0,03
125	0,03
160	0,03
200	0,03
250	0,03
315	0,03
400	0,03
500	0,005
630	0,005
800	0,005
1000	0,005
1250	0,005
1600	0,005
2000	0,005
2500	0,005
3150	0,005
4000	0,005
5000	0,005

Table 4.6: Internal loss factor for each 1/3-octave band, used in modelling the CLT plate.

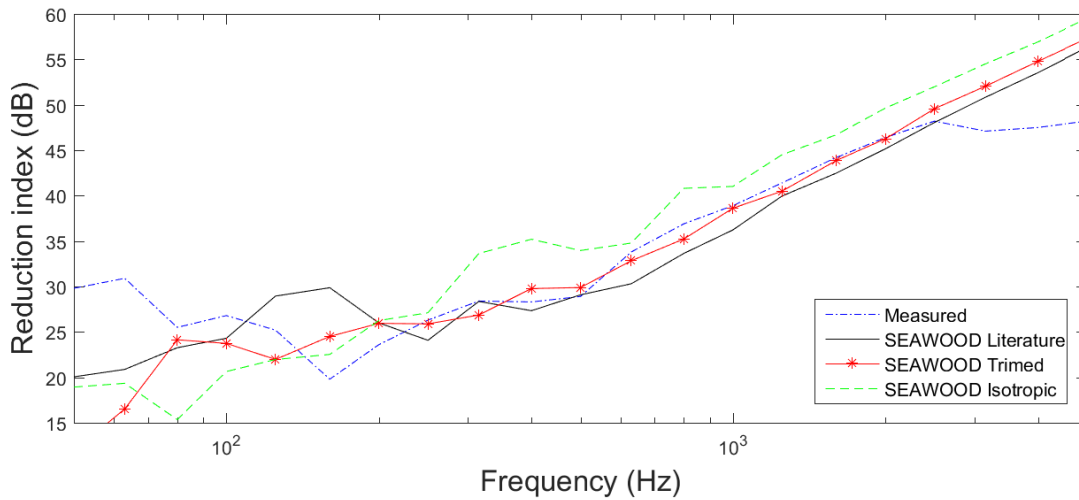


Figure 4.6: Comparison between different internal loss factors of the static uniform CLT320 plate.

5 Validation

This section will present all the different layup cases studied. There will be a method and result part for each case. The method part will show how the model was made and with what material parameters. The results part will show all the calculated data as well as the measurements of the layup. All data in the figures are presented in third octave bands and all plates are considered simply supported. The frequency limit for bending waves on plates and the first resonance of the plate are calculated as shown in section 2.6. The effective quasi longitudinal phase velocity are calculated for CLT plates as shown in equation 2.53. For the weber concrete floor the longitudinal phase velocity used is 3500 m/s and 1490 m/s for the gypsum boards[11], similar values are commonly found in literature. All sources used in the models gave 1W power input to the sending room.

5.1 Simplified SEA model

The simplified model was created in Matlab and calculated as described in section 2.6 and included in figure 5.2. Table 5.1 show the material parameters that were used to make the calculations. The total loss factor for the CLT plate used in the calculations is a lab case approximation. The measurement used as comparison are made in lab conditions so the lab approximation suits fine. Evaluation and comparisons for the model are described more in the next section.

	E_x (Pa)	E_y (Pa)	G_{xy} (Pa)	ρ (kg/m ³)	ν	η_{int}
CLT 140	1,54e10	2,96e8	3,819e9	490	0.44	0.005

Table 5.1: Parameter values for the parameters used in the simplified model with Young's modulus in x and y direction, E_x and E_y . Shears modulus G_{xy} , and Poisson's ratio ν and internal loss factor η_{int}

5.2 CLT140 floor between two rooms

5.2.1 Method

A simulation of a 140 mm thick CLT plate between two rooms was conducted in the SEAWOOD software. The subsystems were set up as shown in figure 5.1 with subsystems 1 and 3 being the rooms and subsystem 2 being the plate. The total loss factor for the rooms are calculated from the reverberation time of the measurement rooms as in equation 2.29.

For the CLT140 plate an investigation regarding the laminate function of the software was conducted. The different type of models are described in section 2.5.7. The laminates were modelled as described in [14] with 5 layers. The outer plates being 4 centimetres thick and 3 inner plates being 2 centimetres thick. The plates were put in a cross pattern with every other plate being turned 90 degrees relative to the layer before it. The resulting material parameters used for the different models can be found in table 5.2.

To find out the impact of the direct transmission between the rooms another simulation was made. When running simulations in the software the direct path is included as described in section 2.5.2. To

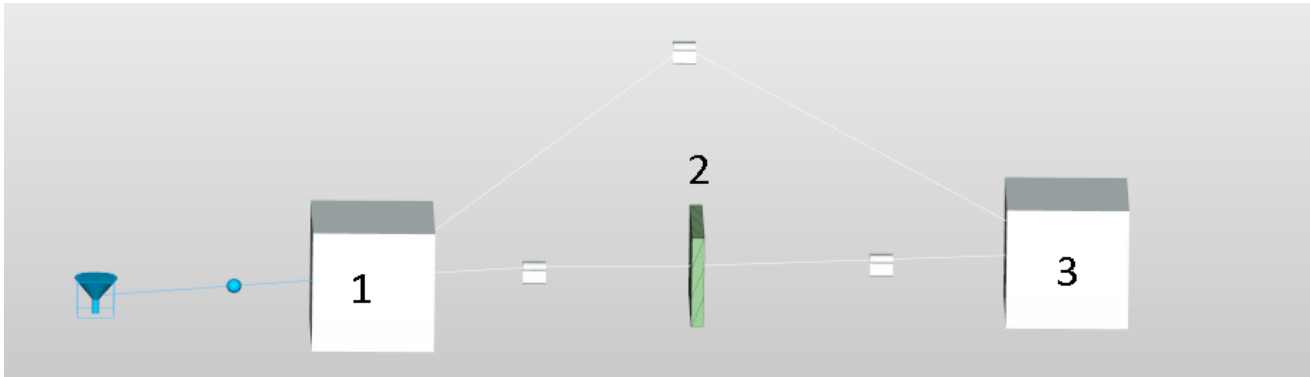


Figure 5.1: Set up of the subsystems in the SEAWOOD software.

	E_x (Pa)	E_y (Pa)	G_{xy} (Pa)	ρ (kg/m ³)	ν_{xy}	ν_{yz}
Uniform	$1,54e10$	$2,96e8$	$3,819e9$	490	0.44	0.64
Dynamic	$1,54e10$	$6,4e9$	$3,819e9$	490	0.028	0.01
Static	$1,54e10$	$6,4e9$	$3,819e9$	490	0.028	0.01

Table 5.2: Parameter values from the software for each laminate type with Young's modulus in x and y direction, E_x and E_y . Shears modulus G_{xy} , and Poisson's ratio for directions ν_{xy} and ν_{yz}

investigate how this direct transmission affected the resulting reduction index, two simulations were made. One with the mass law calculations included and one without them.

5.2.2 Results

In figure 5.2 the resulting reduction index for each of the laminate cases is shown. The measured reduction index as well as the reduction index for the simplified model described in section 2.6 is included. There is not much of a difference between the uniform and dynamic laminates and both corresponds quite well to the measured curve. The dynamic laminate starts out similar to the other laminate types but diverges as the frequency increases. The simplified model is not very accurate in the lower frequency regions but as the frequency increases the curve starts to align with the uniform, static and measured curves. At about 2500 Hz the measured curve starts to form a plateau while the reduction index for the other curves continues to increase with frequency. The calculated effective critical frequency for the simplified model was around 166 Hz. The radiation efficiency of the CLT plate are calculated as described in standard EN 12354-1 using an effective critical frequency. The measurement shows a large dip in the 100-150 Hz region that probably is due to coincidence in the CLT plate. Limitations or inaccuracies in the model might explained the poor fit between the measured and simplified model in the low frequency region. Table 5.3 shows the resulting weighted reduction value and spectral adaptation terms for the

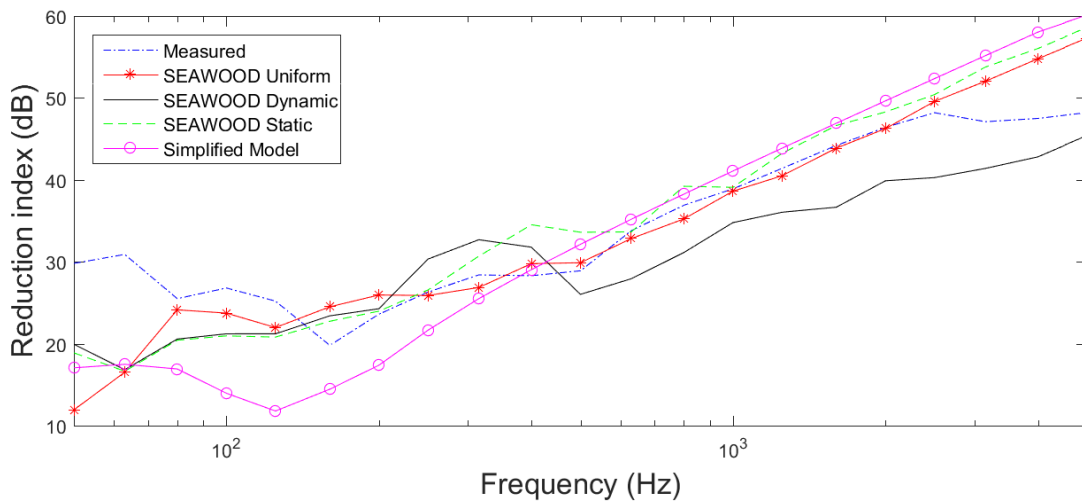


Figure 5.2: Reduction index of a CLT140 plate separating two rooms for different cases.

cases described above. From both the graph and this table it can be concluded that the uniform type of modelling corresponds best to the measured data.

	Measured	SEAWOOD Uniform	SEAWOOD Dynamic	SEAWOOD Static	Simplified Model
R_w	36 dB	36 dB	34 dB	38 dB	33 dB
C	-1 dB	-1 dB	-1 dB	-2 dB	-2
$C_{50-3150}$	-1 dB	-1 dB	-1 dB	-2 dB	-2

Table 5.3: Resulting weighted reduction value R_w for third octave bands ,100-3150 Hz and the spectral adaptation terms C and $C_{50-3150}$ calculated according to ISO 717-1 [16].

In figure 5.3 a comparisons between the resulting reduction index of the CLT140 plate with and

without included mass law calculations is shown. The curves show the CLT140 plate modelled as a uniform section. As expected the reduction index is higher for the lower frequencies when the direct transmission is not included in the model. At about 400 to 1000 Hz the reduction index is slightly lower. This might be due to calculation inaccuracies in the software.

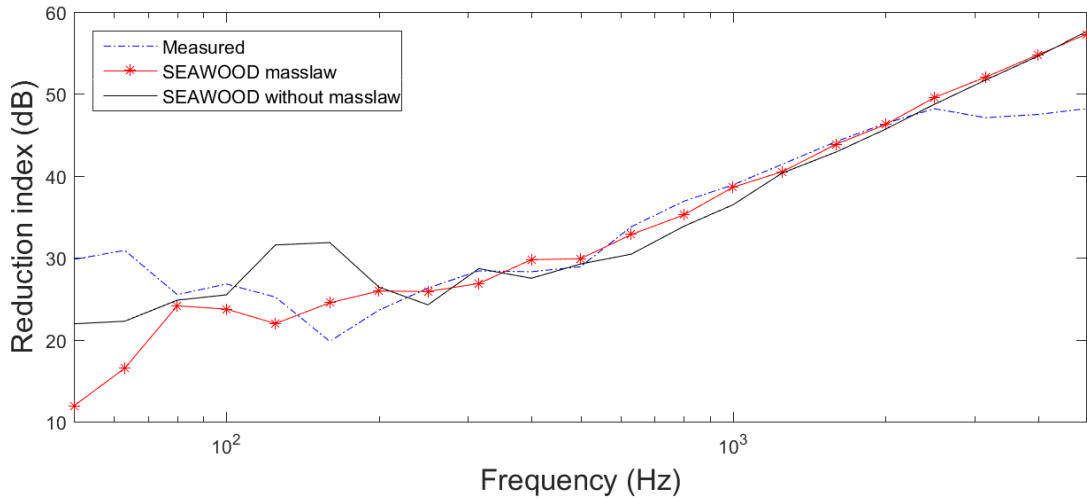


Figure 5.3: Reduction index of the CLT140 plate separating two rooms with and without included mass law calculations

Figure 5.4 shows the number of modes per frequency band for the subsystems. Only the modes per band for one of the rooms are included due to them being identical. The modal numbers are taken from the software and also calculated for the simplified SEA case. The SEAWOOD modal numbers are calculated in the software as described in section 2.1.1. The calculations for room subsystem 1 are made according to equation 2.14 and the calculation for the plate subsystem 2 as according to equation 2.15. The figure shows that the calculated number of modes and the number of modes from the software are similar for the plate subsystem 2. There are some differences probably due to the software including in plane waves in the calculation and also due to the simplification of the calculated mode number. The number of modes for the room subsystem shows the same trend but the number of modes calculated by the software is higher compared to the calculated numbers for the simplified model. This is due to a bug in the software. The modal overlap for the plate subsystem is below 1 for the entire investigated frequency range for both the software and the calculations for the simplified model. For the room subsystem 1 the modal overlap it goes above 1 at 500 Hz for both the software and the calculations for the simplified model.

Table 5.4 shows the calculated upper frequency limit for bending waves on thin plates as well as the calculated first resonance frequency of the CLT140 plate. At higher frequencies it is no longer possible to call it thin any more. As figure 5.2 shows the calculations coincide well with the measurement even beyond the thin plate limit. The first resonance frequency of the plate is calculated to 65 Hz. It is not possible to consider the plate as a subsystems below that.

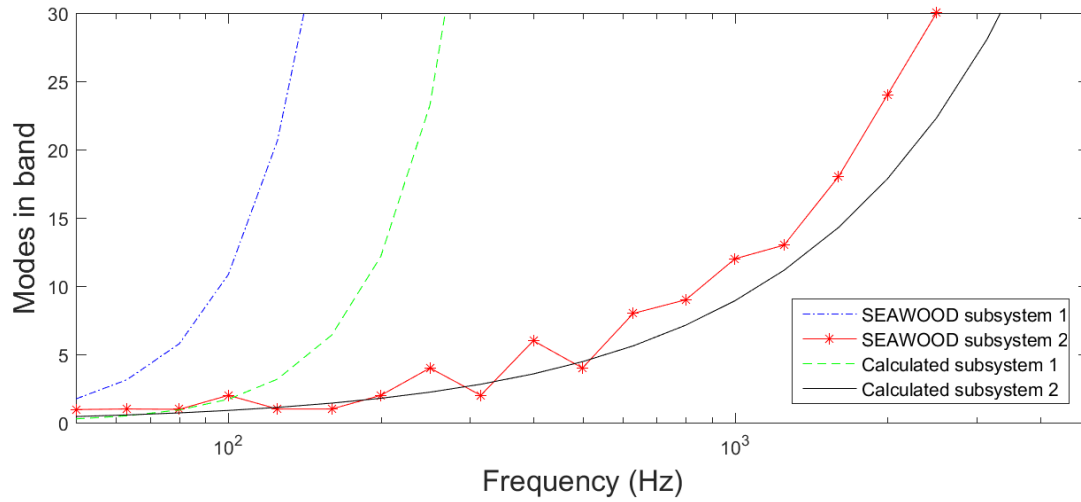


Figure 5.4: Modes per third octave band for the subsystems calculated in SEAWOOD and calculated in Matlab

	$f_{B(thin)}$ (Hz)	$4f_{B(thin)}$ (Hz)	f_{11} (Hz)
CLT140	996	3985	65

Table 5.4: The table shows the thin plate frequency limit for bending waves $f_{B(thin)}$, four times the limit $4f_{B(thin)}$ and the first resonance of the plate f_{11} (Hz for CLT140 plate)

5.3 CLT320 floor between two rooms

5.3.1 Method

In this section the same setup was used as in section 5.2 the only difference is that the CLT plate used are 320 mm thick. The same investigation regarding laminate sections were made. The resulting material parameters for the laminates and uniform sections can be found in table 5.5. The total loss factor for the rooms are calculated from the reverberation time of the measurement rooms as in equation 2.29.

	E_x (Pa)	E_y (Pa)	G_{xy} (Pa)	ρ (kg/m ³)	ν_{xy}	ν_{yz}
Uniform	1,54e10	2,96e8	3,819e9	490	0,44	0,64
Dynamic	1,54e10	6,4e9	3,819e9	490	0,028	0,01
Static	1,54e10	6,4e9	3,819e9	490	0,028	0,01

Table 5.5: Parameter values for each part of the layout with Young's modulus in x and y direction, E_x and E_y . Shears modulus G_{xy} and Poisson's ratio for directions ν_{xy} and ν_{yz}

5.3.2 Results

Figure 5.5 shows the reduction index for the different laminates as well as the measured value. Also included is the reduction index for the calculated simplified model. The curve for the static laminate corresponds quite well at the lower frequencies but starts to deviate more around 900 Hz. The uniform curve compares relatively well to the measured values apart from some larger deviations around 100,400 and 600 Hz. For the dynamic laminate the curve starts off reasonably well but starts to deviate a lot at 400 Hz. At around 3000 Hz it starts to coincide with the measurement but that is probably just a coincidence. The calculated simplified model follows both the static and the uniform curves well but overestimates the reduction index at higher frequencies.

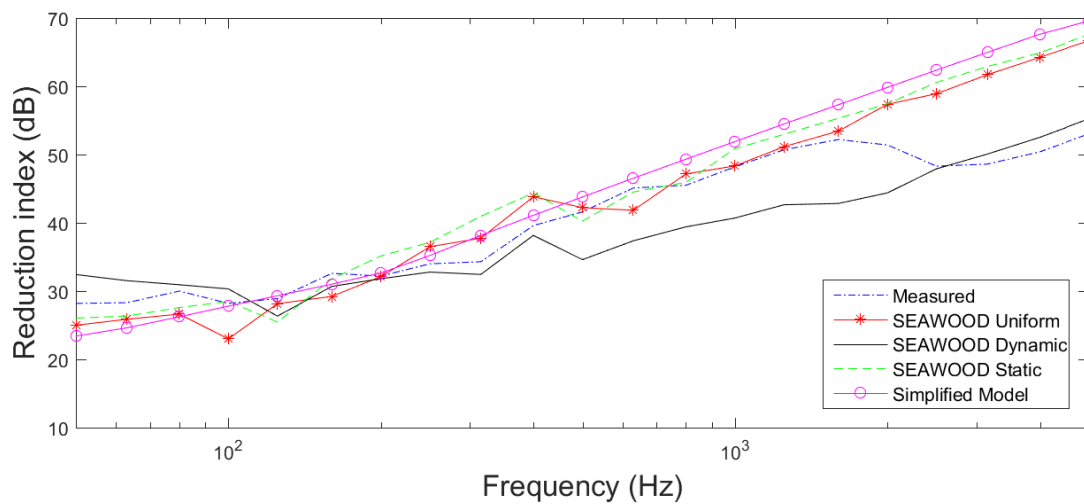


Figure 5.5: Reduction index of a CLT plate separating two rooms.

In table 5.6 the weighted reduction index and spectrum adaptation terms are shown. Between the uniform and measured weighted reduction index there is only a 1 dB difference. Even with the strong deviations mentioned above this makes the uniform section model the most accurate even if the difference between the measurements and the static and simplified models are only 2 dB. When looking at the results of both the CLT 140 and the CLT 320 plate, it becomes clear that the uniform section model is the most accurate one. Therefore all further simulations are made with the CLT plate modelled as a uniform plate.

	Measured	SEAWOOD Uniform	SEAWOOD Dynamic	SEAWOOD Static	Simplified Model
R_w	45 dB	46 dB	41 dB	47 dB	47 dB
C	-1 dB	-2 dB	-1 dB	-2 dB	-2
$C_{50-3150}$	-2 dB	-2 dB	-1 dB	-2 dB	-2

Table 5.6: Resulting weighted reduction value R_w for third octave bands ,100-3150 Hz and the spectral adaptation terms C and $C_{50-3150}$ calculated according to ISO 717-1 [16].

In figure 5.6 a investigation of the direct transfer, as described in section 5.2, is shown. There is not to much difference between the calculations removing the mass law as an influence. The effective critical frequency for the CLT plate is calculated to 72 Hz and that would make the mass controlled area very limited in this case. There should however be a dip in reduction index below the critical frequency range.

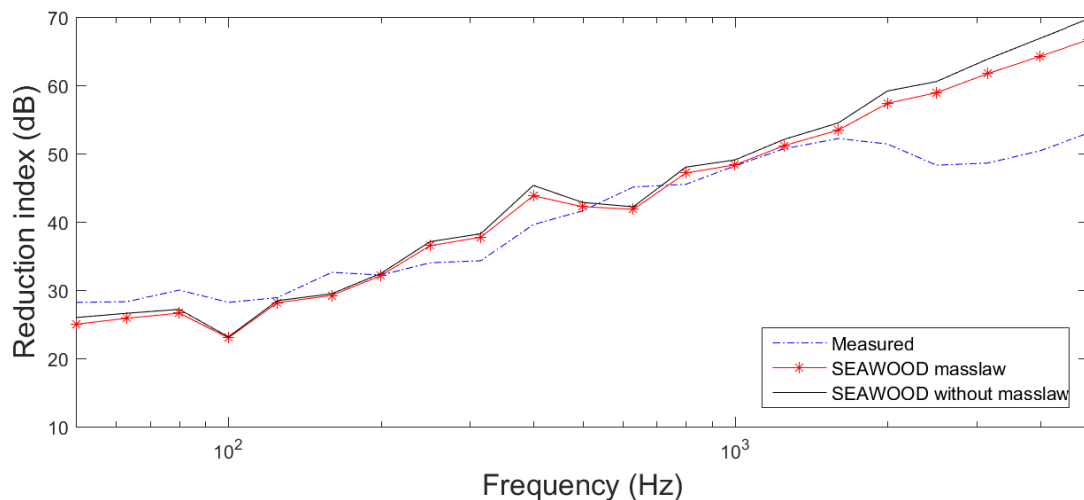


Figure 5.6: Reduction index of the CLT320 plate separating two rooms with and without included mass law calculations

Figure 5.7 shows the number of modes for each third octave band for the subsystem 2 i.e the CLT320 plate. The the rooms are not included here due to them being the same as shown in figure 5.4. The analytically calculated values for the plate are very similar to the values gotten from the software. There are some differences probably to to the software taking in plane waves into account as well as calculating the plate as orothropic. The most important thing about the figure is the low number of modes in the lower frequency bands. Below 1000 Hz the number of modes per band are less than 5 and below 100 Hz less

than 1. The modal overlap was calculated to be below 1 for all the frequency bands. Combined with the low number of modes in the frequency bands the accuracy of the SEA model could be questioned. Even though the reduction index curves and weighted reduction index indicate that the modal fit reasonably well, this may be just a coincidence.

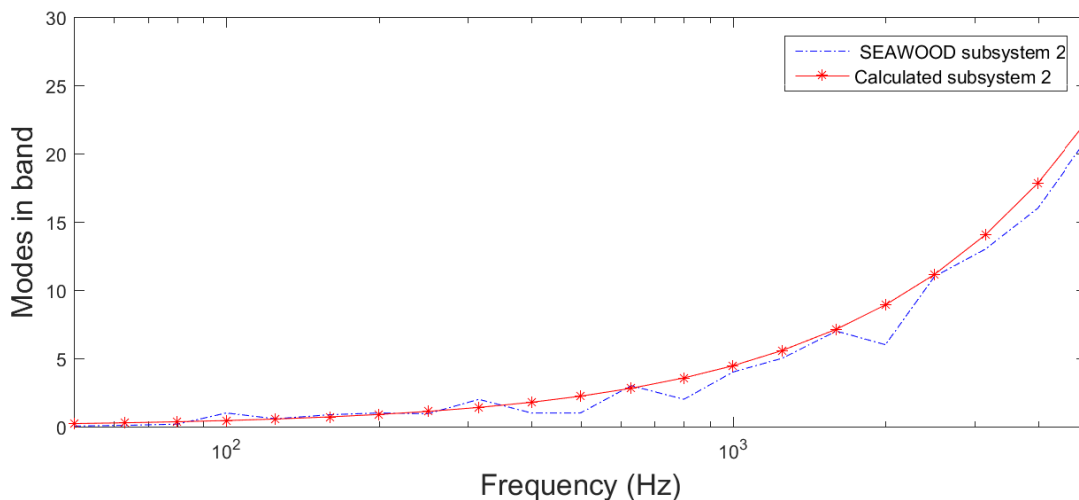


Figure 5.7: Reduction index of a CLT plate separating two rooms.

Table 5.7 shows the calculated upper frequency limit for bending waves on thin plates as well as the calculated first resonance frequency of the CLT320 plate. At higher frequencies it is no longer possible to call it thin any more. The frequency limit for CLT320 plate is in the lower region. Even with the four times the limit assumption it is low. Figure 5.5 shows that at around 1600 Hz the measured curve starts to plateau. This is about the same as the $4f_{B(thin)}$ frequency. This will be more closely discussed in the discussions section of this thesis. The first resonance frequency of the plate is calculated to 85 Hz. It is not possible to consider the plate as a subsystem below that frequency.

	$f_{B(thin)}$ (Hz)	$4f_{B(thin)}$ (Hz)	f_{11} (Hz)
CLT320	435	1743	85

Table 5.7: The table shows the thin plate frequency limit for bending waves $f_{B(thin)}$, four times the limit $4f_{B(thin)}$ and the first resonance of the plate f_{11} (Hz) for CLT320 plate)

5.4 Assembly of CLT140 with impact sound insulation and Weber floor

5.4.1 Method

This layout consisted of a combination of a concrete floor with a wooden CLT plate and added impact sound insulation as shown in figure 5.8. The material data used for the Weber concrete floor and impact sound insulation layer was taken from the software and can be found in table 5.8. Full material properties for these materials can be found in Appendix A. Two different internal loss factor for the weber concrete was tested. One calculated as approximated by Craik as described in equation 2.32 which translates to an internal loss factor of 0,015. The other was from report [17] and gives an internal loss factor of 0.01. The total loss factor for the rooms are calculated from the reverberation time of the measurement rooms as in equation 2.29.



Figure 5.8:
 1)60 mm Weber floor
 2)20 mm Isover TDTP20
 3)140 mm CLT140 board

	E_x (Pa)	E_y (Pa)	G_{xy} (Pa)	ρ (kg/m ³)	ν_{xy}	ν_{yz}
CLT140	1,54e10	2,96e8	3,819e9	490	0,44	0,64
Weber 318	1,04e11	1,04e11	1,00e10	2300	0,37	0,37
Isover TDPT impact sound insulation	5,2e6	5,2e6	5,2e6	184	0,01	0,01

Table 5.8: Parameter values for each part of the layout with Young's modulus in x and y direction, E_x and E_y . Shears modulus G_{xy} and Poisson's ratio for directions ν_{xy} and ν_{yz}

The layout was modelled in the software as four different subsystems as shown in figure 5.9.

Subsystems 1 and 4 being the sending and receiving rooms with a direct connection between them. Subsystem 2 being the concrete Weber floor. Subsystem 3 being the CLT plate with an added trim layer consisting of the impact sound simulation. Subsystem 2 and 3 are connected with a line connection with the same length as the longest side of the plate.

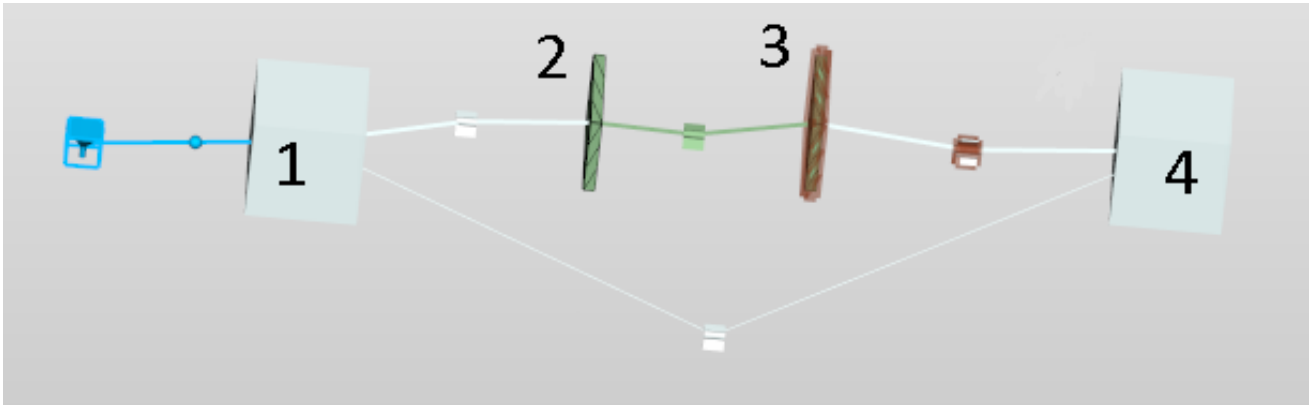


Figure 5.9: SEA subsystems as modelled in the software.

5.4.2 Results

Figure 5.10 shows the resulting reduction index curves for the measured layup and simulated layup from the software. There is also a reduction index curve where the internal loss factor of the Weber concrete floor are calculated with an approximation by Craik, as shown in equation 2.32, instead of the material data from the software. The figure shows that the SEAWOOD calculations corresponds well to the measured values for almost the entire investigated frequency range even in the lower frequencies. The comparison between the SEAWOOD curve and the curve with an internal loss factor calculated according to Craik shows quite a big difference mostly around about 130 to 1800 Hz. It still corresponds reasonably well to the measurement however.

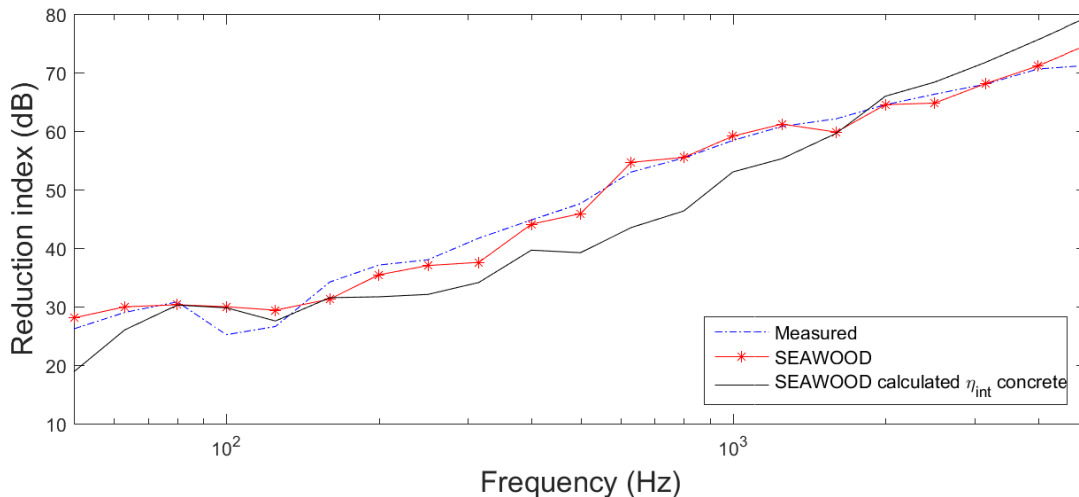


Figure 5.10: Comparison between the measured and SEAWOOD calculated reduction index curves. The SEAWOOD curves compare a common loss factor for concrete with a calculated estimation suggested by Craik.

Table 5.9 shows the weighted reduction index and the spectral adaptation terms for the reduction index curves. It also shows that the simulation from SEAWOOD corresponds well to the measured

values. The weighted reduction index for the calculated internal loss factor of the concrete plate does not correspond as well due to the deviation as mentioned before.

	Measured	SEAWOOD	SEAWOOD calculated η_{omt} concrete
R_w	49 dB	49 dB	45 dB
C	-2 dB	-2 dB	-2 dB
$C_{50-3150}$	-2 dB	-2 dB	-2 dB

Table 5.9: Resulting weighted reduction value R_w for third octave bands ,100-3150 Hz and the spectral adaptation terms C and $C_{50-3150}$ calculated according to ISO 717-1 [16].

In figure 5.11 two reduction index curves are compared. The curves are the same as the SEAWOOD curve in figure 5.10 except for one curve that shows direct connection between the sending and receiving room without masslaw calculations, so all sound are assumed to travel through the layup. The figure shows that there is a small difference below 80 Hz there are also differences at around 700 Hz and also above 2000 Hz. If the direct transmission between the rooms were more prominent the should be a dip in the reduction index for the lower frequency regions. The critical frequency of the concrete plate is calculated to 127 Hz. This might explain why there is so little difference when not including the direct transmission.

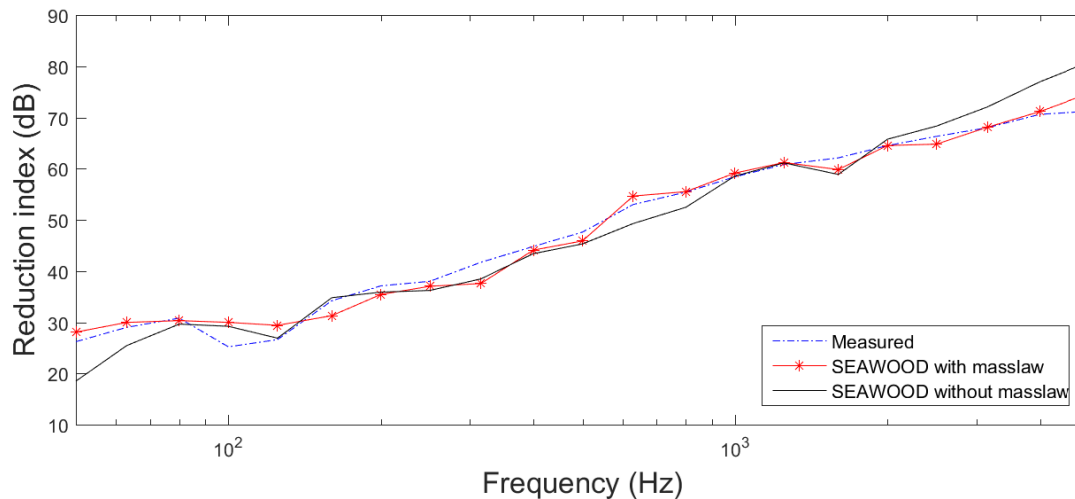


Figure 5.11: Comparisons of reduction index curves with and without direct transmission between the rooms.

In figure 5.12 the modes in each frequency band for the concrete and the CLT plates are shown. The rooms are the same size as the previous layouts so only the CLT plate and the concrete are shown. There are few modes below 100 Hz and the mode count only starts to increase above 1000 Hz. The modal overlap for the rooms are the same as in the previous layouts. For the plates the modal overlap is below 1 for all the investigated frequencies. This could mean that the model is not very accurate below about 1000 Hz. However the simulations corresponds very well with the measured values.

Table 5.10 shows the calculated upper frequency limit for bending waves on thin plates as well as the

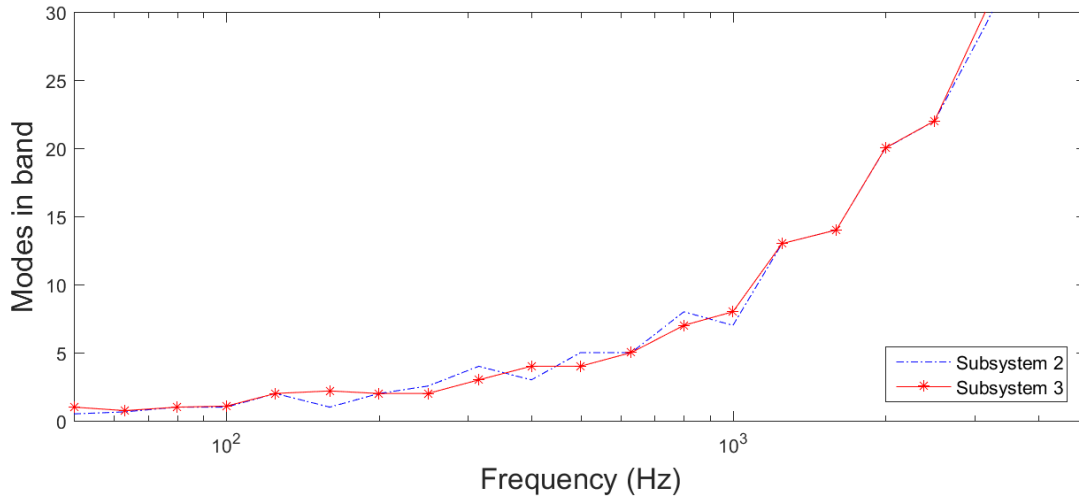


Figure 5.12: Number of modes for each third octave band for the subsystems included in the model.

calculated first resonance frequency of the plates included in the SEA model. Figure 5.10 shows that even though the frequency limit is 996 Hz for the CLT and 2917 Hz for the Weber concrete floor the calculations coincides well with the measurements. This suggests that the frequency limit times four is an acceptable upper frequency limit for bending waves on thin plates. It is also interesting the the measurements starts to plateau around the $4f_{B(thin)}$ for the CLT plate.

	$f_{B(thin)}$ (Hz)	$4f_{B(thin)}$ (Hz)	f_{11} (Hz)
CLT140	996	3985	56
Weber	2917	11167	51

Table 5.10: The table shows the thin plate frequency limit for bending waves $f_{B(thin)}$, four times the limit $4f_{B(thin)}$ and the first resonance of the plate f_{11} for the Weber floor and CLT140

5.5 Two CLT plates, mineral filled cavity, with and without added gypsum boards

5.5.1 Method

This layout consists of two parts. The layout consists of two CLT plates separated by a cavity filled with mineral wool. In one case there is also an addition of four gypsum boards between the cavity and a CLT plate. This is shown in figure 5.13. The total loss factor for the sending and receiving rooms are calculated from the reverberation time approximated as 2 seconds for all frequencies as in equation 2.29.

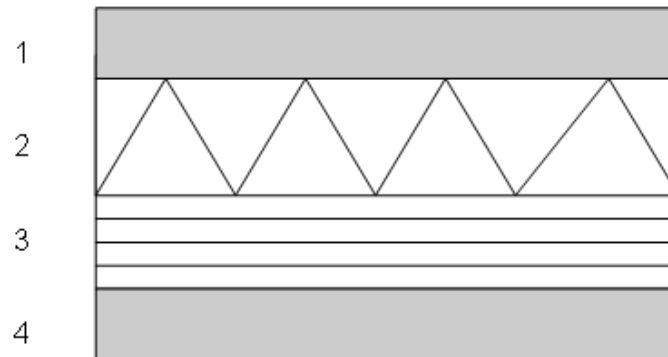


Figure 5.13:
 1) CLT
 2) Cavity with mineral wool
 3) 4 layers of 12.5 mm gypsum boards
 4) CLT

In table 5.11 the material data for the plates are shown. The material data for the gypsum boards are for an isotropic plate and taken from [18] but with an internal loss factor of 0,01.

	E_x in Pa	E_y in Pa	G_{xy} in (Pa)	ρ in (kg/m ³)	ν_{xy} -	ν_{yz} -
CLT	1,54e10	2,96e8	3,819e9	490	0,44	0,64
Gypsum boards	7e9	7e9	2,69e9	1200	0,3	0,3

Table 5.11: Parameter values for each part of the floor layout with Young's modulus in x and y direction, E_x and E_y . Shears modulus G_{xy} and Poisson's ratio for directions ν_{xy} and ν_{yz}

Table 5.12 shows some of the properties for the mineral wool used in the cavity. The full material data can be found in appendix A.

Figure 5.14 shows the SEA model as set up in the software. Subsystem 1 and 6 are sending and receiving rooms. Subsystem 2 are one of the CLT plates. Subsystem 3 are the cavity filled with mineral wool. Subsystem 4 is the four gypsum boards created as a static laminate. The gypsum boards are

	ρ in kg/m ³	Flow resistivity in N s/m ⁴
Mineral wool	50 dB	60000 dB

Table 5.12: Data mineral wool used in the layup with, density ρ and Flow resistivity kg/m³.

connected with a line connection to the other CLT plate. The connection length are the same as the longest side of the plate. In the case where the gypsum boards are not present the subsystem 5 is directly connected to the cavity subsystem 3. In this case the measurements was supposed to have been made with the sending and receiving rooms structurally separated. Therefore it is assumed that all direct transmission goes through the cavity.

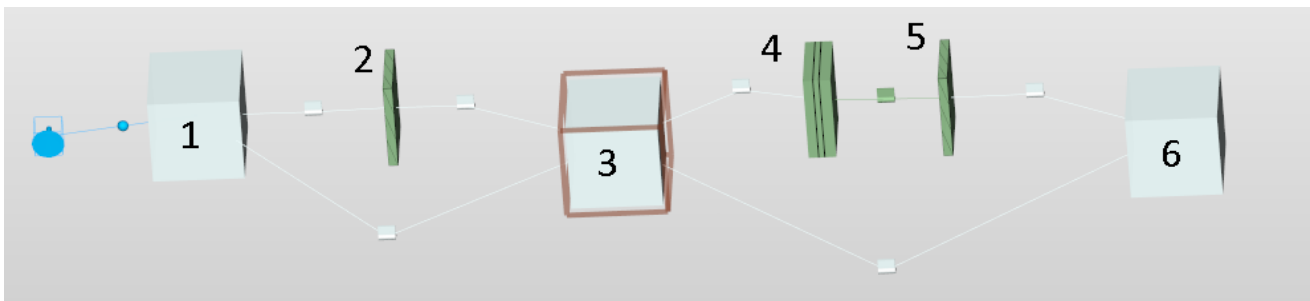


Figure 5.14: SEA subsystems as modelled in the software.

5.5.2 Results

In figure 5.15 the resulting reduction index for both the case with gypsum boards and the case without are shown in comparison to the measured data. The reduction index of the case with the gypsum boards corresponds well in the frequency region between 100 and 800 Hz. In the case without the gypsum boards the SEAWOOD calculation are fairly accurate even in the lower frequency regions but it starts to deviate at about 1400 Hz where both the measured curves reaches a very similar plateau. The SEAWOOD prediction is also lower in the 100 to 650 Hz region for the case without gypsum boards.

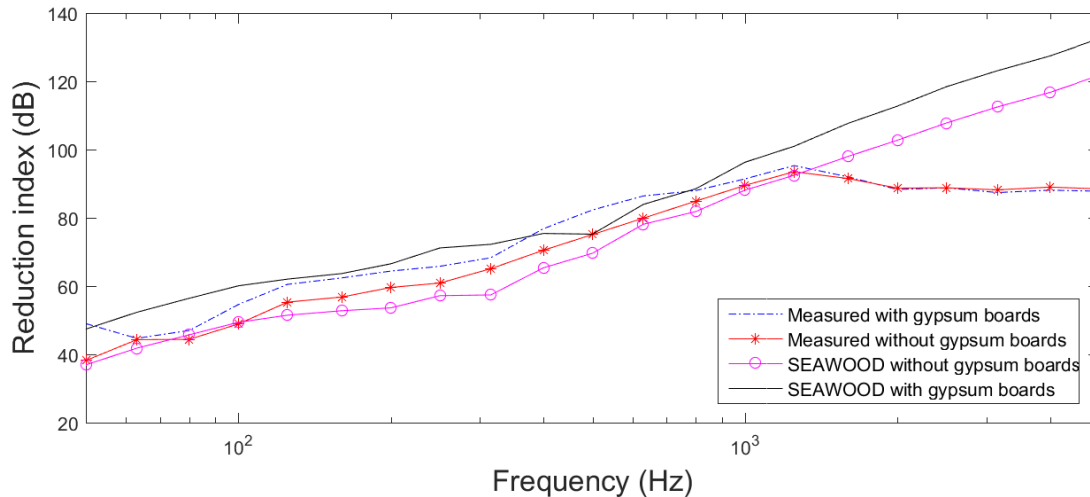


Figure 5.15: Comparison between the measured and SEAWOOD calculated reduction index curves for both cases.

Table 5.13 shows the weighted reduction index and the spectral adaptation terms for the reduction index curves of the case with gypsum plates. The weighted reduction index is fairly close to that of the measurement.

	Measured with gypsum	SEAWOOD with gypsum
R_w	79 dB	81 dB
C	-2 dB	-2 dB
$C_{50-3150}$	-5 dB	-3 dB

Table 5.13: Resulting weighted reduction value R_w for third octave bands ,100-3150 Hz and the spectral adaptation terms C and $C_{50-3150}$ calculated according to ISO 717-1 [16].

Table 5.14 shows the weighted reduction index and the spectral adaptation terms for the case without gypsum plates. The weighted single values and spectral adaptation terms are slightly different. The cause for this are the deviations between the measured and SEAWOOD calculations in the whole frequency where the weighted terms are calculated. The exception being the region around 1000 Hz where the curves coincide.

	Measured without gypsum	SEAWOOD without gypsum
R_w	74 dB	69 dB
C	-2 dB	-1 dB
$C_{50-3150}$	-4 dB	-2 dB

Table 5.14: Resulting weighted reduction value R_w for third octave bands ,100-3150 Hz and the spectral adaptation terms C and $C_{50-3150}$ calculated according to ISO 717-1 [16].

In figure 5.16 a comparison between the calculations with and without direct transmission are shown. The figure is for the case with the gypsum boards added. There is clearly a mass dominated region below about 300 Hz. There is also a difference above 1000 Hz.

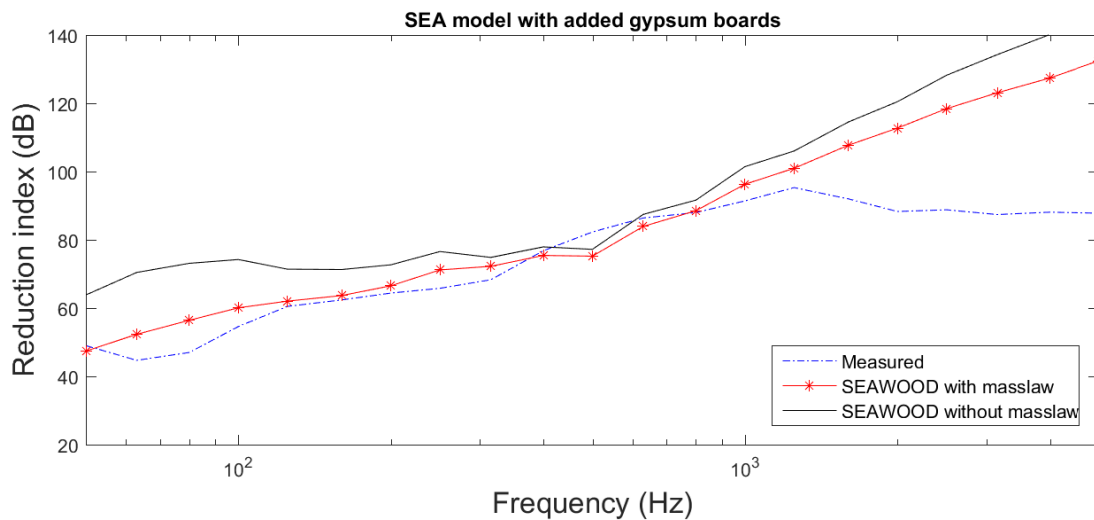


Figure 5.16: Comparisons of reduction index curves with and without direct transmission between the rooms for the case with the added gypsum boards.

A similar result can be seen in the figure 5.17. It is also shown in the case without the added gypsum boards. There the mass dominated region is a bit lower in frequency and starts around 180 Hz though. There are also the same difference above 1000 Hz where the reduction index becomes higher the there is not direct transmission.

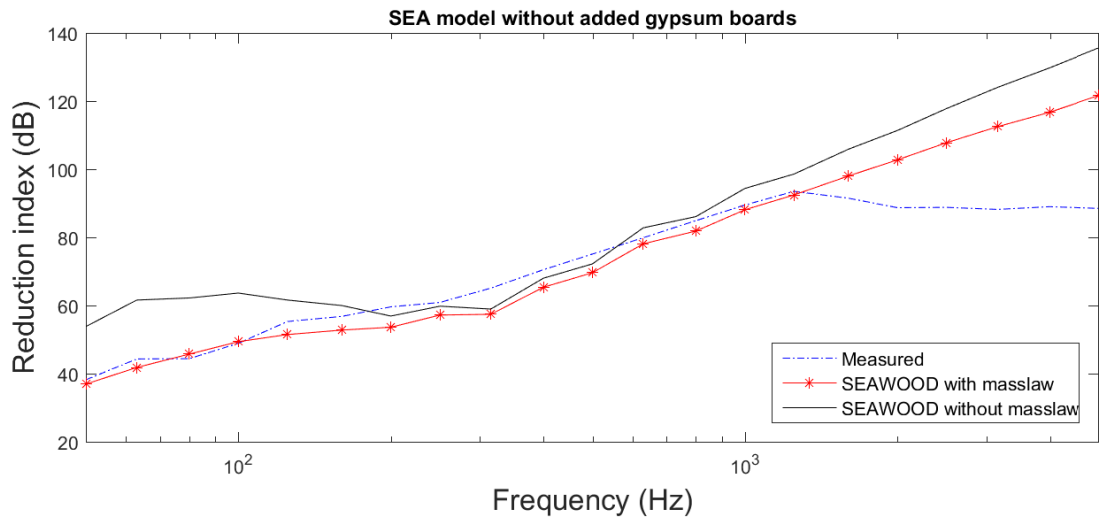


Figure 5.17: Comparisons of reduction index curves with and without direct transmission between the rooms for the case without the gypsum boards.

The number of modes in each third octave band for each subsystem are shown in figure 5.18. The subsystem number corresponds to the ones in figure 5.14. Subsystem 1 and 6 are the same so only number 1 will be shown. It is clear that the mode count for all involved subsystems are very low below 100 Hz. The mode count for the CLT plates increases the least with frequency.

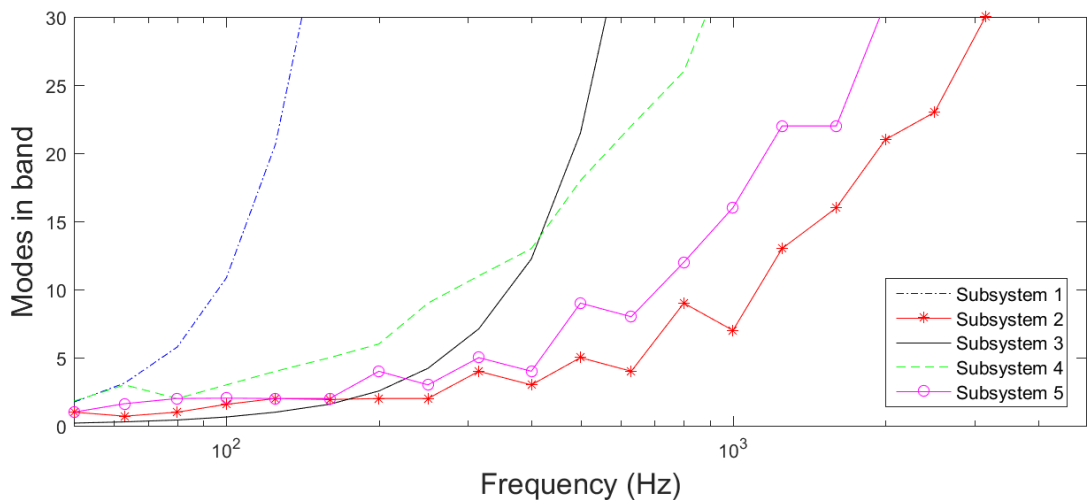


Figure 5.18: Number of modes in each third octave band for each subsystem included in the model.

Table 5.15 shows at what frequency the modal overlap factor of each subsystem is above 1. For both CLT plates it is below 1 for the whole investigated frequency region and very high for the gypsum boards. This combined with low modal count of the plate subsystems may explain why the SEA model deviates from the measurements.

Table 5.16 shows the calculated upper frequency limit for bending waves on thin plates as well as the calculated first resonance frequency of the plates included in the SEA model. The frequency limit for

Subsystem	1	2	3	4	5
MOF>1	400 Hz	-	200 Hz	4000Hz	-

Table 5.15: Frequencies where the modal overlap factor are above 1 for each subsystem included in the model.

the CLT plates are quite low in frequency but the calculations and measurements coincide fairly well up until 1400 Hz where the measurement plateau. The measured curves starts to plateau quite far below the $4f_{B(thin)}$ range for each plate subsystem. Below the first resonance frequency of each plate the plate can not be modelled as a subsystem.

	$f_{B(thin)}$ (Hz)	$4f_{B(thin)}$ (Hz)	f_{11} (Hz)
CLT Subsystem 2	871	3486	64
CLT Subsystem 5	1394	5578	40
Gypsum boards	1490	5960	11

Table 5.16: The table shows the thin plate frequency limit for bending waves $f_{B(thin)}$, four times the limit $4f_{B(thin)}$ and the first resonance of the plate f_{11} (Hz) for the CLT and gypsum plates.)

5.6 CLT plate with foam insulation

5.6.1 Method

This wall layup consists of a CLT plate with an added layer of foam insulation as well as a silicone plaster finish as shown in figure 5.19. The silicone layer will not be included into the SEA model due to difficulties modelling it. This will affect the sound insulation prediction. The total loss factor for the rooms are calculated from the approximated reverberation time of 2 seconds of the measurement rooms, as in equation 2.29. The material data for the foam layer and CLT plate can be found in table 5.17. The



Figure 5.19:
1)Silicone plaster
2)Foam insulation
3)CLT

material characteristics are taken from the software library and the full material data can be found in appendix A.

	E_x in Pa	E_y in Pa	G_{xy} in (Pa)	ρ in (kg/m ³)	ν_{xy} -	ν_{yz} -
CLT	1,54e10	2,96e8	3,819e9	490	0,44	0,64
Plastic Foam	1,43e5	1,43e5	2,3e7	31	0,3	0,3

Table 5.17: Parameter values for each part of the layup with Young's modulus in x and y direction, E_x and E_y . Shears modulus G_{xy} and Poisson's ratio for directions ν_{xy} and ν_{yz}

Figure 5.20 shows the subsystems included in the SEA model. Subsystem 1 and 3 are the sending and receiving rooms. Subsystem 2 are the CLT plate with the foam insulation added as a trim layer.

5.6.2 Results

Figure 5.21 shows the resulting reduction index curves for the measured data compared to SEAWOOD calculations. When comparing the measured reduction index to the SEAWOOD calculation it can be seen the it does not correspond well. It is similar at frequencies below 200 Hz but the the software overestimates the reduction index and after that is underestimates it above 500 Hz. Not including the silicone plaster layer makes the calculated results less accurate. The silicone plaster layer acts as a mass against the stiffness of the foam layer. This creates a mass spring mass behaviour that can be

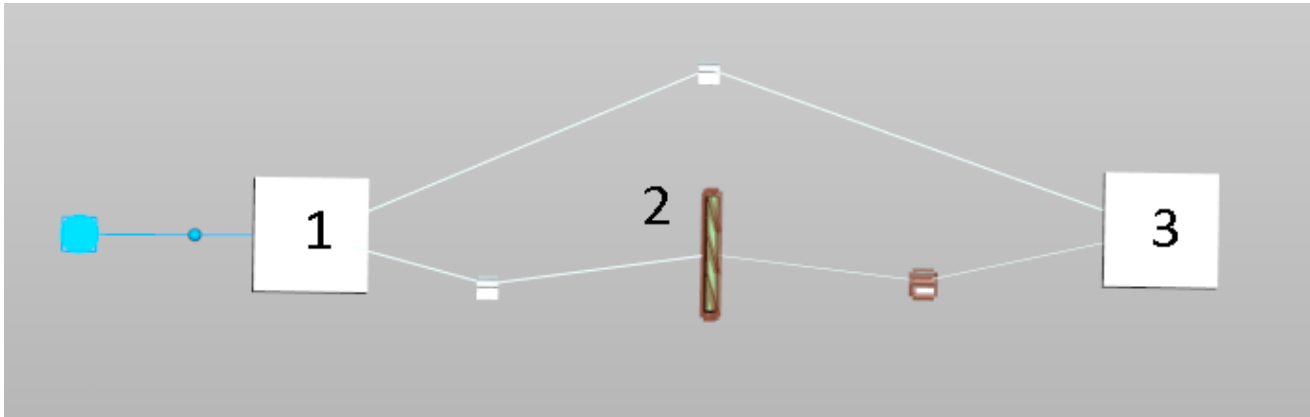


Figure 5.20: Subsystem setup for the SEA model in the software.

seen measured result. At 300 Hz there is a breathing frequency and above that there is an increase by 6dB/octave.

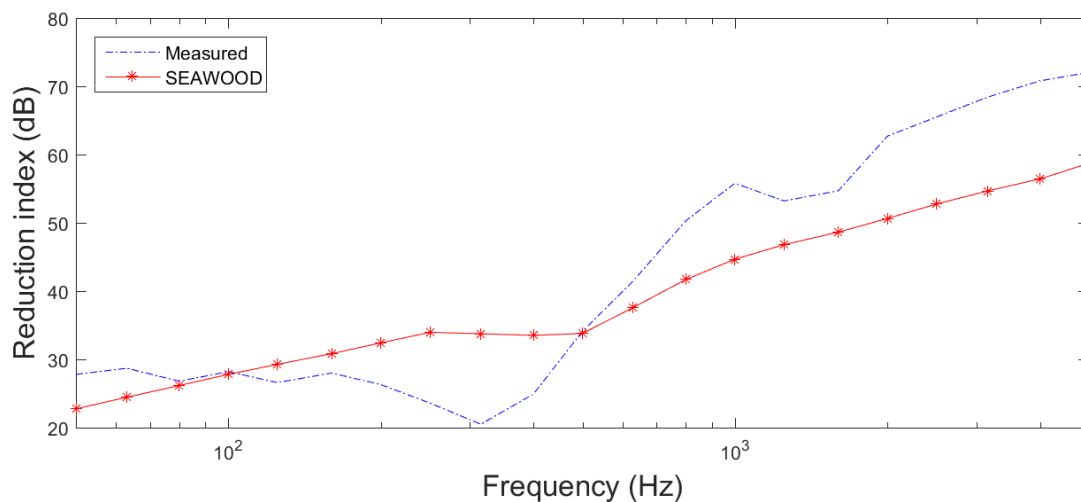


Figure 5.21: Comparison between the measured and SEAWOOD calculated reduction index curves.

Table 5.13 shows the weighted reduction index and the spectral adaptation terms for the reduction index curves. Due to the big difference between the SEAWOOD calculations and the measurements there is a relatively big difference in weighted values and spectral adaptation terms.

	Measured	SEAWOOD
R_w	36 dB	42 dB
C	-2 dB	-1 dB
$C_{50-3150}$	-2 dB	-8 dB

Table 5.18: Resulting weighted reduction value R_w for third octave bands ,100-3150 Hz and the spectral adaptation terms C and $C_{50-3150}$ calculated according to ISO 717-1 [16].

For the direct transmissions shown in figure 5.22 it can clearly be seen that there is a mass dominated region at frequencies below 300 Hz but there is also a very large increase in reduction index at frequencies above 1000 Hz. This may be due to how the software calculated the transmission loss through the foam insulation trim layer on the CLT plate.

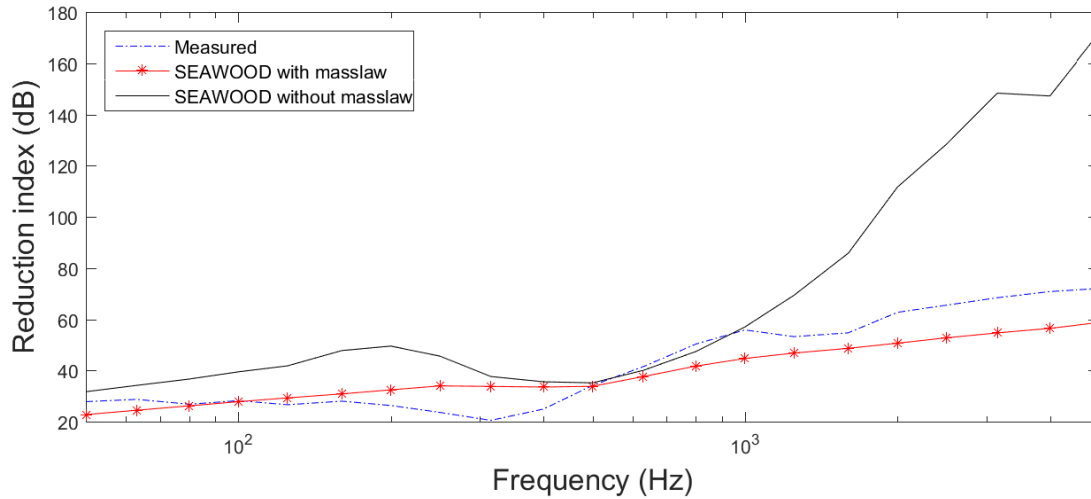


Figure 5.22: Comparisons of reduction index curves with and without direct transmission between the rooms.

In figure 5.23 the number of modes in third octave band are shown for the included subsystems. Subsystem 1 and 3 are the same so only subsystem 1 will be shown. As usual the mode count for the CLT plate are low. Also the Modal overlap factor is below 1 for the whole frequency region for the CLT plate subsystem while for the sending and receiving rooms it is above 1 for frequencies above 630 Hz. The low number of modes in the interested frequency ranges as well as the poor modal overlap may be a cause for the poor result in this case. There is also a strong possibility that the foam insulation material parameters used in the simulations were not a good representation of the actual material. This may also be a explanation for the poor result.

Table 5.19 shows the calculated upper frequency limit for bending waves on thin plates as well as the calculated first resonance frequency of the CLT plate included in the SEA model. Both the thin plate frequency limit and the first resonance frequency of the CLT plate indicated that the plate should be able to be modelled as a subsystem fairly well based on these theories. The large difference between the measured data and the calculations are probably more due to the uncertainty of the material parameters of the plastic foam trim layer as mentioned above.

	$f_{B(thin)}$ (Hz)	$4f_{B(thin)}$ (Hz)	f_{11} (Hz)
CLT subsystem 2	1550	6199	34

Table 5.19: The table shows the thin plate frequency limit for bending waves $f_{B(thin)}$, four times the limit $4f_{B(thin)}$ and the first resonance of the plate f_{11} (Hz) for CLT subsystem 2)

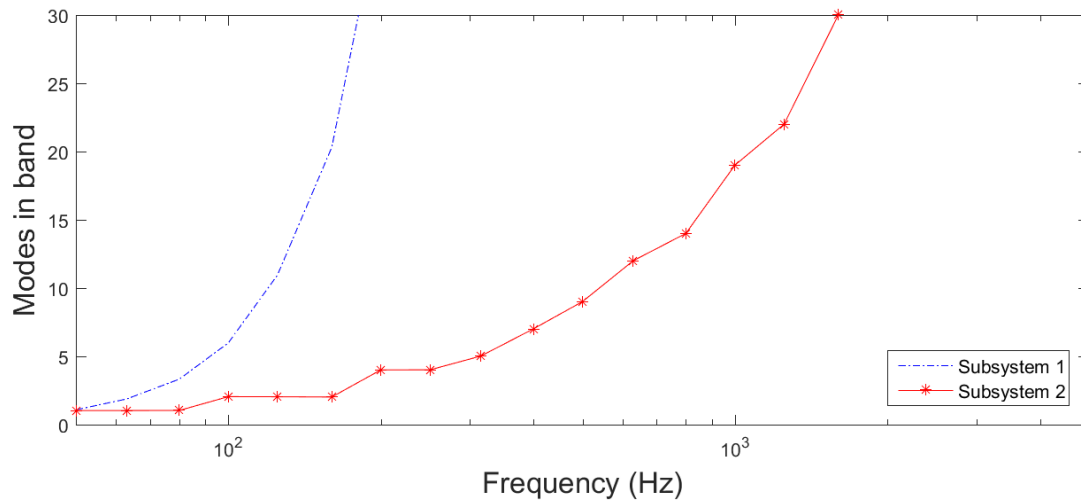


Figure 5.23: Number of modes in each third octave band for each subsystem included in the model.

5.7 CLT plate with foam insulation, mineral filled cavity and two gypsum boards.

5.7.1 Method

This wall layup consists of a CLT plate with an added layer of foam insulation as well as a silicone plaster finish as shown in figure 5.24. The silicone layer will not be included into the SEA model due to difficulties modelling it as a separate subsystem. There are also a cavity filled with mineral wool as well an assembly of two gypsum boards. The total loss factor for the rooms are calculated from the approximated reverberation time of 2 seconds of the measurement rooms, as in equation 2.29.

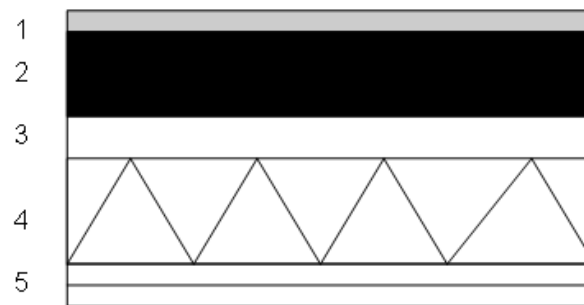


Figure 5.24:
 1)Silicone plaster
 2)Foam insulation
 3)CLT
 4)Cavity with Mineral wool insulation
 5)Two Gypsum boards

Table 5.20 and 5.21 shows the material parameters for each part of the layup. The full material properties for the foam insulation and mineral wool can be found in appendix A. The gypsum boards have an internal loss factor of 0,01.

	E_x in Pa	E_y in Pa	G_{xy} in (Pa)	ρ in (kg/m ³)	ν_{xy} -	ν_{yz} -
CLT	1,54e10	2,96e8	3,819e9	490	0,44	0,64
Gypsum boards	7e9	7e9	2,69e9	1200	0,3	0,3
Plastic Foam	1,43e5	1,43e5	2,3e7	31	0,3	0,3

Table 5.20: Parameter values for each part of the layup with Young's modulus in x and y direction, E_x and E_y . Shears modulus G_{xy} and Poisson's ratio for directions ν_{xy} and ν_{yz}

In figure 5.25 the subsystems included in the SEA model are shown. Subsystems 1 and 5 are the sending and receiving rooms. Subsystem 2 are the two gypsum boards. Subsystem 3 are the cavity filled with mineral wool. The mineral wool are added as a trim layer to the cavity. Subsystem 4 are the CLT

	ρ in kg/m ³	Flow resistivity in N s/m ⁴
Mineral wool	50 dB	60000 dB

Table 5.21: Material data for the mineral wool used in the layup with, density ρ and Flow resistivity kg/m³.

plate with the foam insulation added as a trim layer. To create as simple model as possible it is assumed that all direct transmission goes through the cavity as the rooms are structurally separated.

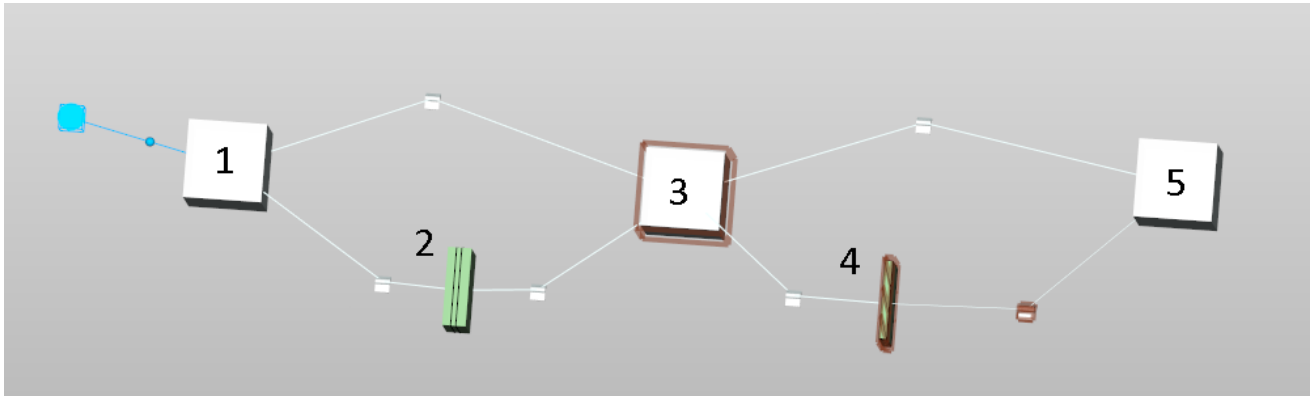


Figure 5.25: Numbered subsystems as modeled in the SEAWOOD software

5.7.2 Results

In figure 5.26 a comparison between the measured and SEAWOOD calculated reduction index curves. SEAWOOD seems to overestimate the reduction index for the frequency region below 800 Hz. Around 1000 Hz both curves start to coincide but the measurement starts to deviate soon after as the SEAWOOD curve continues to rise.

Table 5.22 shows the weighted reduction index and the spectral adaptation terms for the reduction index curves. There is quite a few decibels different between the values. Most of it could be attributed to the large different in the frequency range of 180 to 600 Hz region as well as the deviation in the higher frequencies.

	Measured	SEAWOOD
R_w	53 dB	61 dB
C	1 dB	-5 dB
$C_{50-3150}$	-4 dB	-12 dB

Table 5.22: Resulting weighted reduction value R_w for third octave bands ,100-3150 Hz and the spectral adaptation terms C and $C_{50-3150}$ calculated according to ISO 717-1 [16].

Figure 5.27 shows a comparison of the SEAWOOD calculated curves with and without masslaw

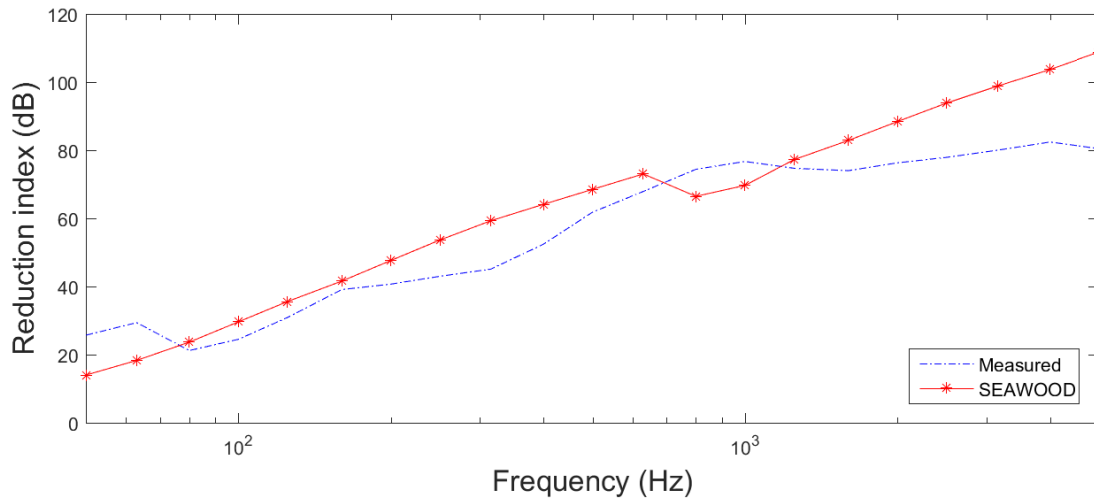


Figure 5.26: Comparison between the measured and SEAWOOD calculated reduction index curves.

calculation of the direct transmission. Below 800 Hz there is a large increase in reduction index when the direct transmission is removed. There is also a large increase above 800 Hz. This may be due to how the software calculates the transmission loss through the foam insulation layer.

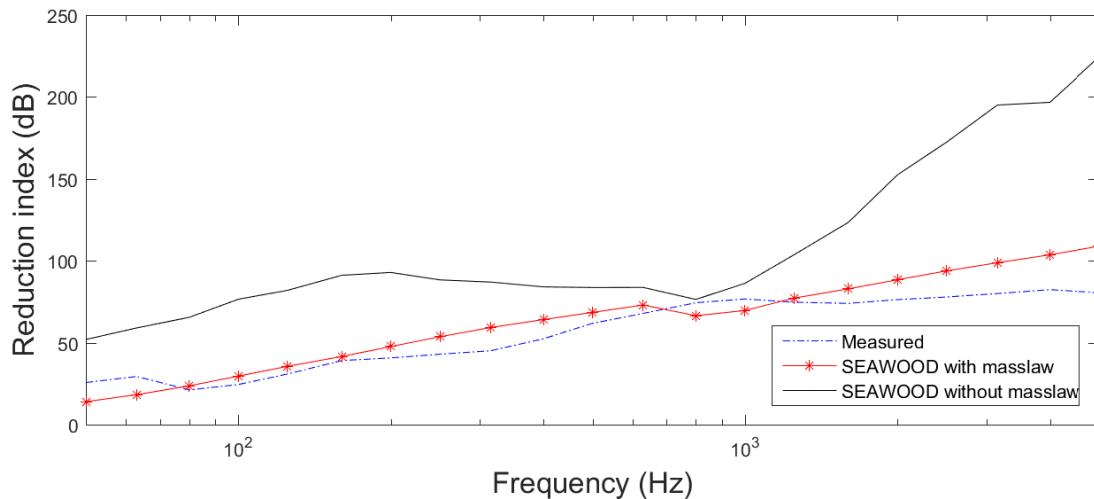


Figure 5.27: Comparisons of reduction index curves with and without direct transmission between the rooms.

In figure 5.28 the number of modes in each third octave band is shown for each subsystem included in the model. The room subsystems 1 and 5 are include in the previous layup as they are the same the will not be shown here. The gypsum board subsystem 2 contain quite many modes per band even at lower frequencies while the cavity subsystem 3 and the CLT subsystem 4 contains few.

Table 5.23 shows at what frequency the modal overlap factor becomes larger than 1 for each subsystem.

The low modal overlap and the relativity low number of modes in the subsystems may affect the accuracy of the SEA model. Also the plastic foam material parameters may not be representative of the

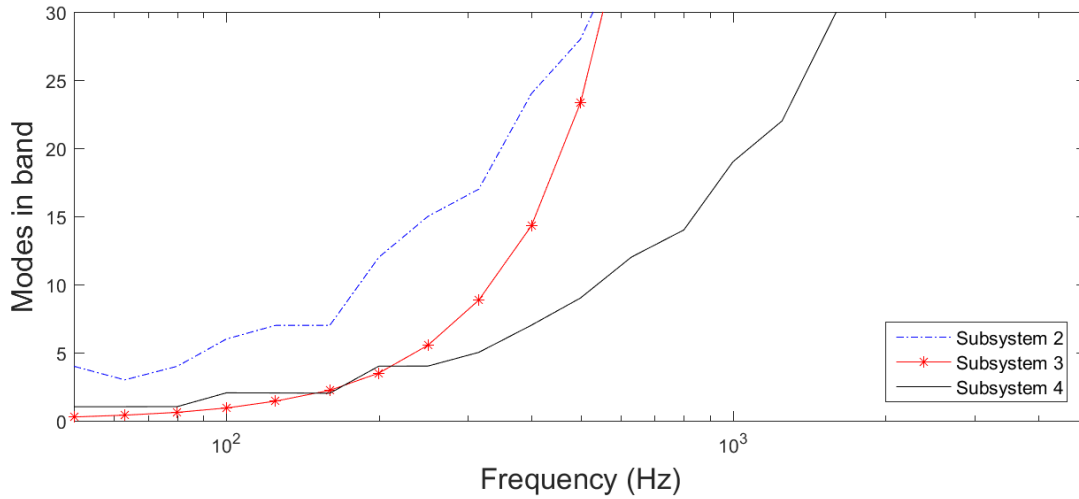


Figure 5.28: Number of modes in each third octave band for each subsystem included in the model.

Subsystem	2	3	4	-	-
MOF>1	2500 Hz	200 Hz	- Hz		-

Table 5.23: Frequencies where the modal overlap factor are above 1 for each subsystem included in the model.

real world material.

Table 5.24 shows the calculated upper frequency limit for bending waves on thin plates as well as the calculated first resonance frequency for the plates included in the SEA model. The thin plate limit for both plate types are fairly high. The first resonance frequency shows that the plates can possibly be modelled as subsystems as it is below the lowest frequency band investigated.

	$f_{B(thin)}$ (Hz)	$4f_{B(thin)}$ (Hz)	f_{11} (Hz)
CLT Subsystem 2	1550	6199	36
Gypsum boards	2483	9933	7

Table 5.24: The table shows the thin plate frequency limit for bending waves $f_{B(thin)}$, four times the limit $4f_{B(thin)}$ and the first resonance of the plate f_{11} (Hz for the CLT and gypsum plates.)

5.8 CLT with a gypsum board separated by a mineral wool filled cavity and a added mineral wool insulation layer.

5.8.1 Method

For this wall layup the construction consisted of a gypsum board. A cavity filled with mineral wool supported by fixed wooden studs. After the cavity a CLT plate was placed with a layer of mineral wool insulation and a plaster finish. To simplify the model the plaster layer will not be included as a subsystem. The total loss factor for the rooms are calculated from the approximated reverberation time of 2 seconds of the measurement rooms, as in equation 2.29.

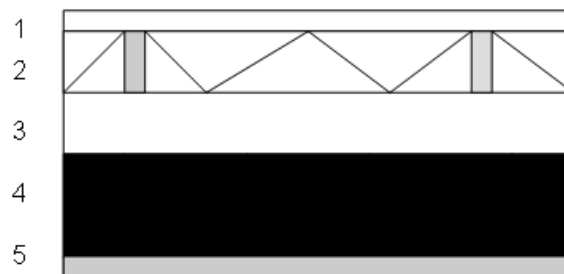


Figure 5.29: 1)Gypsum board
2)Cavity with fixed wooden studs and mineral wool
3)CLT
4)Mineral wool insulation
5)Plaster

The properties for the materials used in the layup are presented in table 5.25 and 5.26. The gypsum boards have an internal loss factor of 0,01.

	E_x in Pa	E_y in Pa	G_{xy} in (Pa)	ρ in (kg/m ³)	ν_{xy} -	ν_{yz} -
CLT	1,54e10	2,96e8	3,819e9	490	0,44	0,64
Gypsum boards	7e9	7e9	2,69e9	1200	0,3	0,3

Table 5.25: Parameter values for each part of the layup with Young's modulus in x and y direction, E_x and E_y . Shears modulus G_{xy} and Poisson's ratio for directions ν_{xy} and ν_{yz}

	ρ in kg/m ³	Flow resistivity in N s/m ⁴
Mineral wool	50	60000

Table 5.26: Material data for the mineral wool used in the layup with, density ρ and Flow resistivity kg/m³.

The SEA model with the appointed subsystems are presented in figure 5.30. Subsystem 1 and 5 are the sending and receiving rooms. Subsystem 2 is gypsum board. Subsystem 3 is the cavity with mineral wool modelled as a trim layer. Subsystem 4 are the CLT plate with the mineral wool insulation added as a trim layer. The model assumes that all direct transmission goes through the cavity.

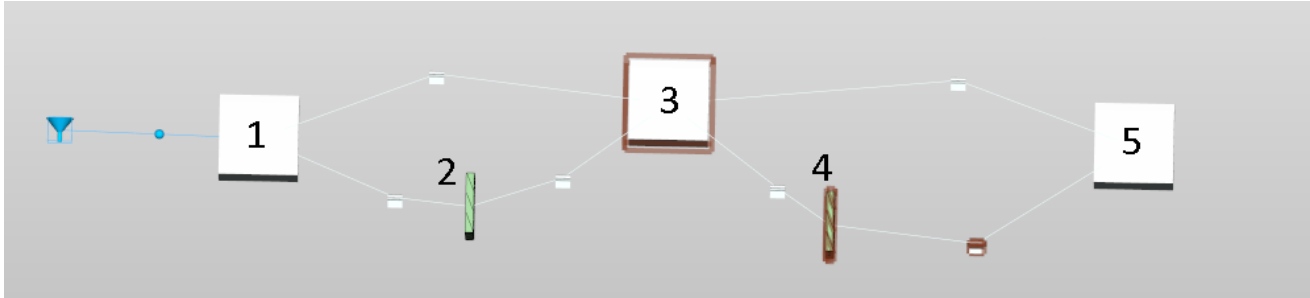


Figure 5.30: Numbered subsystems that is included in the SEAWOOD model.

5.8.2 Results

Figure 5.31 shows a comparison of the reduction index curves for the measured data and the calculations from SEAWOOD. For almost the whole investigated frequency range the software overestimates the reduction index. The exception being at about 1800 Hz where the SEAWOOD curve dips down below the measured and then continues to raise again. A possible explanation for this may be that the mineral wool insulation added as trim layer in the model is not modelled correctly. There may be too much reduction from these elements in both the cavity and on top of the CLT plate compared to the real life case.

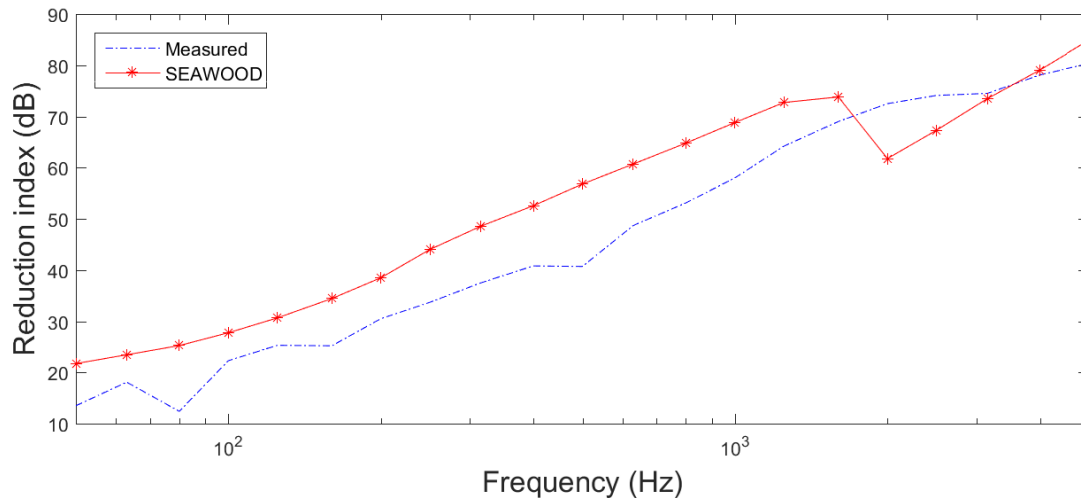


Figure 5.31: Comparison between the measured and SEAWOOD calculated reduction index curves.

Table 5.27 shows the weighted reduction index and the spectral adaptation terms for the reduction index curves. There is a large difference between the measurements and the SEAWOOD calculations for both the weighted reduction index as well as the adaptation terms. When looking at figure 5.31 this result is not surprising due to the large overestimation from the SEAWOOD software.

	Measured	SEAWOOD
R_w	45 dB	54 dB
C	-1 dB	-3 dB
$C_{50-3150}$	-4 dB	-13 dB

Table 5.27: Resulting weighted reduction value R_w for third octave bands ,100-3150 Hz and the spectral adaptation terms C and $C_{50-3150}$ calculated according to ISO 717-1 [16].

Figure 5.27 shows the difference when including direct transmission or not, as calculated by mass law, into the system. When removing the direct transmission the reduction index rose to almost 20 dB above the original values. This is probably due to the calculated transmission loss from the trim layers affecting the the whole frequency range.

In figure 5.33 the number of modes in each third octave band are shown. For the sending room

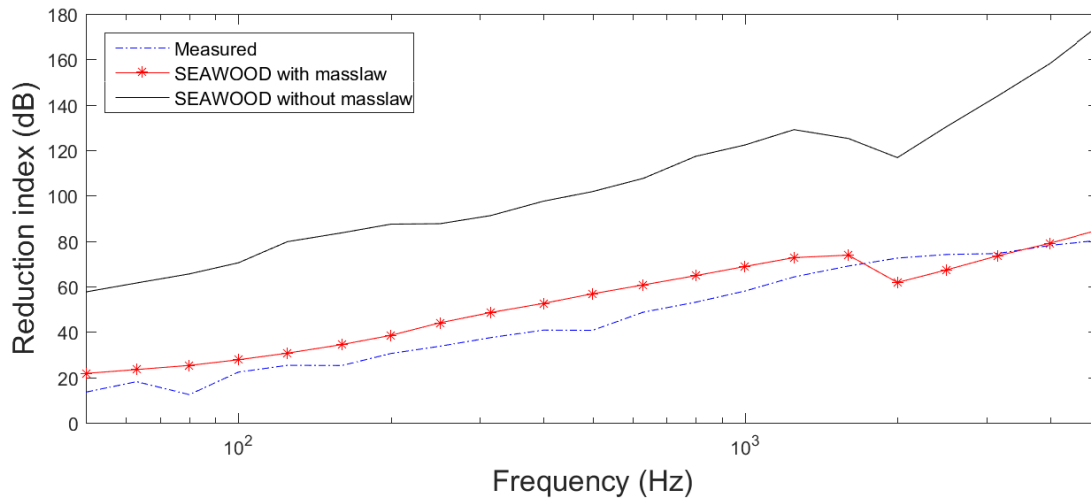


Figure 5.32: Comparisons of reduction index curves with and without direct transmission between the rooms.

subsystem 1, the gypsum plate subsystem 2 have quite many modes per band even in the lower frequencies. Below 100 Hz there are few modes in each band for all the subsystems except the gypsum plate subsystem 2. The mode count for the cavity subsystem 3 starts to become high at about 300 Hz. The mode count in the CLT plate subsystem 4 is low below 1000 Hz and then starts to increase beyond that.

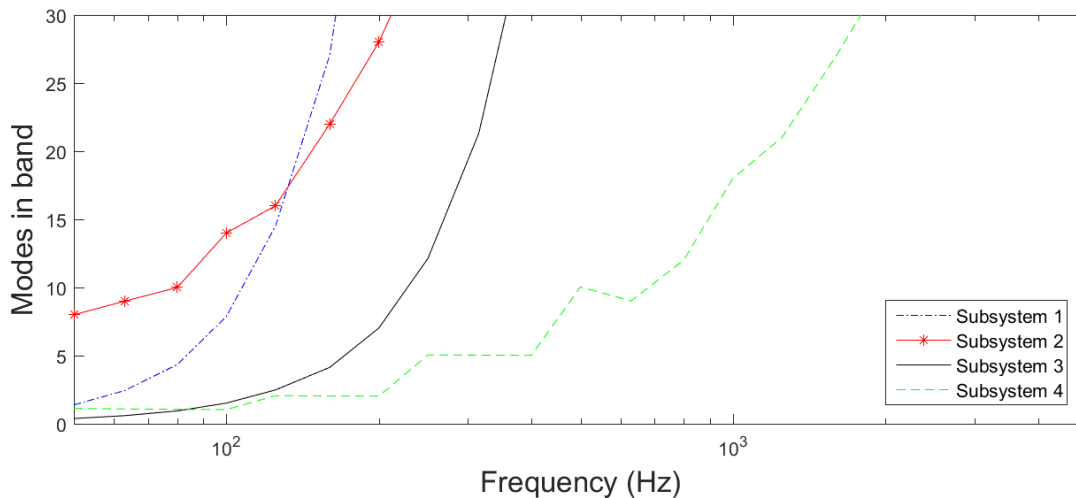


Figure 5.33: Number of modes in each third octave band for each subsystem included in the model.

Table 5.28 shows at what frequency the modal overlap factor becomes larger than 1 for each of the subsystem. It is noteworthy that as usual the CLT plate modal overlap does not go past 1 for the entire frequency range.

The relative high number of modes in each third octave band for almost all of the subsystems indicates even with the low modal overlap that the model should be fairly accurate. The difference between the measurement and the SEAWOOD calculations is probably due to how the mineral wool is implemented

Subsystem	1	2	3	4
MOF>1	500 Hz	1000	1250 Hz	-

Table 5.28: Frequencies where the modal overlap factor are above 1 for each subsystem included in the model.

in the model and the affect it has on the reduction index. Table 5.29 shows the calculated upper frequency limit for bending waves on thin plates as well as the calculated first resonance frequency for the plates included int he SEA model. The thin plate limit for the CLT plate is fairly high and very high for the thin gypsum plate. The low first resonance frequency shows that the plates can possibly be modelled as subsystems as it is below the lowest frequency band investigated.

	$f_{B(thin)}$ (Hz)	$4f_{B(thin)}$ (Hz)	f_{11} (Hz)
CLT Subsystem 4	1550	6199	40
Gypsum board	5960	23840	3

Table 5.29: The table shows the thin plate frequency limit for bending waves $f_{B(thin)}$, four times the limit $4f_{B(thin)}$ and the first resonance of the plate f_{11} (Hz for the CLT and gypsum plates.)

5.9 CLT between two cavities with mineral wool and CW and CD profiles and added gypsum boards

This wall layup consist of two gypsum boards in each end of the layup. The CLT plate is located in-between the gypsum separated by two cavities filled with mineral wool. The cavities also contains metal rails called CD and CW profiles. The layup is shown in figure 5.34. The total loss factor for the rooms are calculated from the approximated reverberation time of 2 seconds of the measurement rooms, as in equation 2.29.

5.9.1 Method

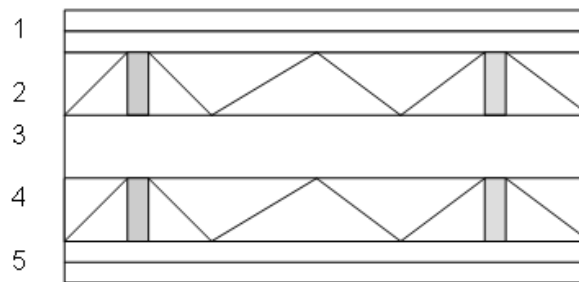


Figure 5.34:

- 1) Two Gypsum boards
- 2) Cavity with CD-profile and mineral wool
- 3) CLT
- 4) Cavity with CW-profile and mineral wool
- 5) Two Gypsum boards

The properties for the materials used in the layup are presented in table 5.30 and 5.31. The gypsum boards have an internal loss factor of 0,01.

	E_x in Pa	E_y in Pa	G_{xy} in (Pa)	ρ in (kg/m ³)	ν_{xy} -	ν_{yz} -
CLT	$1,54e10$	$2,96e8$	$3,819e9$	490	0.44	0.64
Gypsum boards	$7e9$	$7e9$	$2,69e9$	1200	0.3	0.3

Table 5.30: Parameter values for each part of the layup with Young's modulus in x and y direction, E_x and E_y . Shears modulus G_{xy} and Poisson's ratio for directions ν_{xy} and ν_{yz}

	ρ in kg/m ³	Flow resistivity in N s/m ⁴
Mineral wool	50 dB	60000 dB

Table 5.31: Material data for the mineral wool used in the layup with, density ρ and Flow resistivity kg/m³.

The SEA model with the appointed subsystems are presented in figure 5.35. Subsystem numbers 1 and 7 are the sending and receiving room subsystems. Subsystems 2 and 6 are the two gypsum plates modelled as a static laminate. Subsystems 3 and 5 are the cavity subsystems filled with mineral wool. The metal CD and CW profiles are not included in the cavities due to problems modelling them. To try to include the coupling of the CD and CW profiles, connections between the gypsum plates and the CLT subsystem 4 was added. The different connection type are further explained in section 2.5.3. The direct transmission path was added through the cavities.

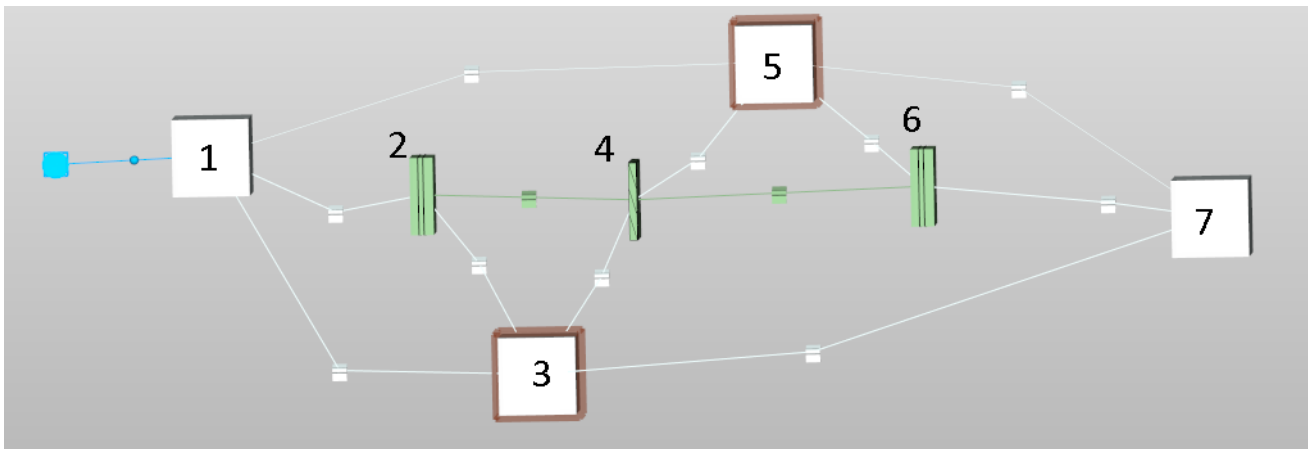


Figure 5.35: Numbered subsystems that is included in the SEAWOOD model.

5.9.2 Results

Figure 5.36 shows a comparison of the reduction index curves between the measurements and the SEAWOOD calculations. The different connection types refers to how the plates are coupled together and at about 200 Hz they start to differentiate a lot from each other. When using point connection the software underestimates the reduction index and when there is no connection between the CLT and the gypsum plates the software overestimates the reduction index. When using the point connection the SEAWOOD calculations fits the closest to the measurements but this may just be a coincidence. Further investigation may be needed to find the best way to model these types of layouts.

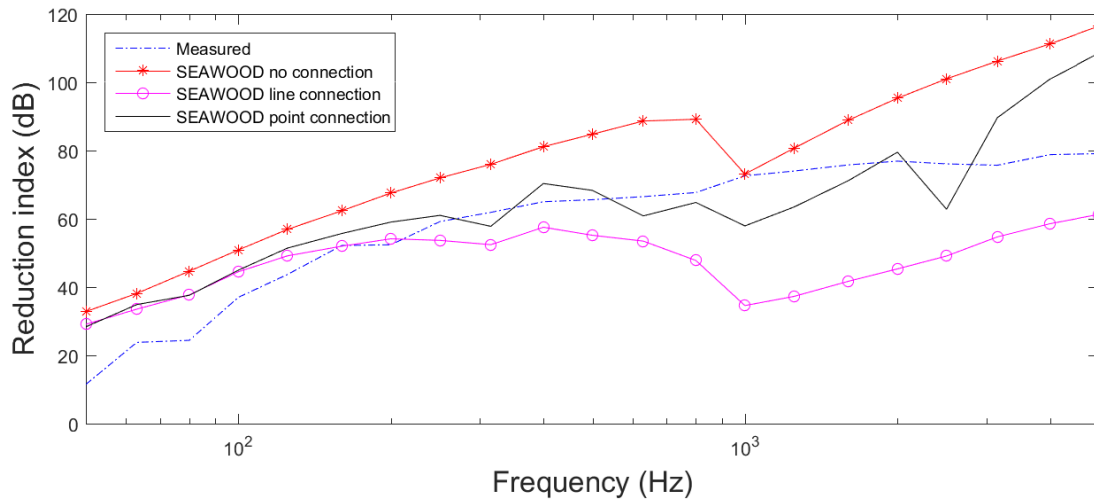


Figure 5.36: Comparison of the reduction index for SEAWOOD calculations with different plate connections and measurements, in third octave bands.

Table 5.32 shows the weighted reduction index and the spectral adaptation terms for the reduction index curves. As seen in figure 5.36 the point connection type is the closest to the weighted single values and adaptation terms for the measurements.

	Measured	Point connection	Line connection	No connection
R_w	67 dB	64 dB	43 dB	79 dB
C	-4	-1 dB	-2 dB	-3 dB
$C_{50-3150}$	-17	-14 dB	7 dB	-30 dB

Table 5.32: Resulting weighted reduction value R_w for third octave bands ,100-3150 Hz and the spectral adaptation terms C and $C_{50-3150}$ calculated according to ISO 717-1 [16].

In figure 5.37 the point connection reduction index curve from figure 5.36 is shown with the direct transmission path removed. There is a small increase in reduction index the lowest frequency band but the largest difference is between 300 and 5000 Hz. This may indicate that the SEAWOOD model is not correctly modelled.

In figure 5.38 the number of modes in each third octave band for each subsystem is shown. The

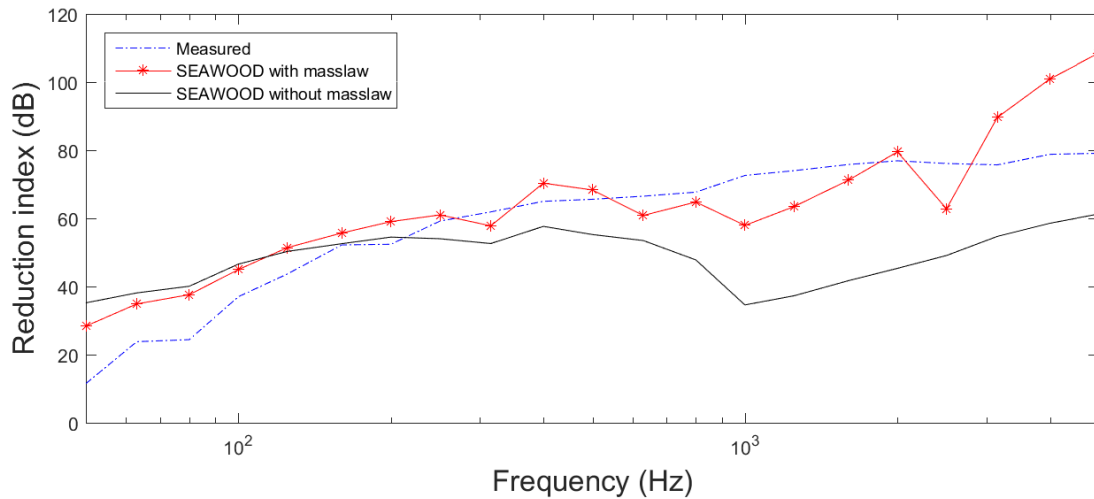


Figure 5.37: Comparisons of reduction index curves with and without direct transmission trough the cavities.

sending and receiving room is the same as the previous layout and can be found in table 5.28. The gypsum plate subsystems 2 and 6 are the same so only one will be included. The gypsum plate subsystem has some modes per band below 100 Hz but the mode count starts to really increase above 300 Hz. The cavity subsystems 3 and 5 are the same so only one will be included. The cavity subsystem has few modes below 200 Hz but starts to increase above 200 Hz. The CLT plate subsystem has low modal count below 1000 Hz and only goes above 30 modes in each band above 2000 Hz.

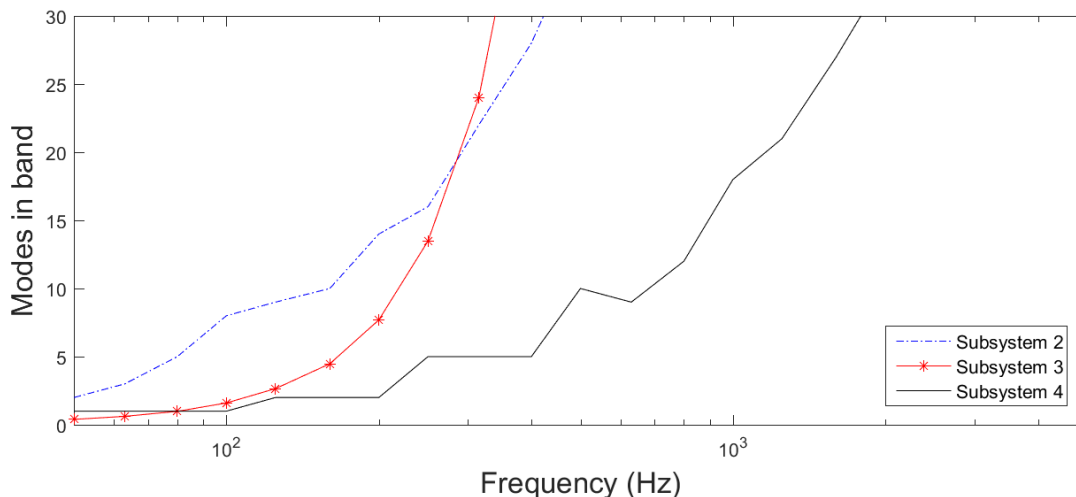


Figure 5.38: Number of modes in each third octave band for each subsystem included in the model.

Table 5.33 shows at what frequency the modal overlap factor becomes larger than 1 for each of the subsystem.

When looking at the mode count and the overlap for the subsystems it is possible that accuracy of the SEA model is not very good for lower frequencies. However when using the model with point

Subsystem	2	3	4
MOF>1	2000 Hz	400	-

Table 5.33: Frequencies where the modal overlap factor are above 1 for each subsystem included in the model.

connections between the plates the SEAWOOD calculations seems to compare relatively well with the measurement. This may be a coincidence though due to the other uncertainties of the model mentioned earlier. Table 5.34 shows the calculated upper frequency limit for bending waves on thin plates as well as the calculated first resonance frequency for the plates included in the SEA model. The thin plate limit for the CLT plate is fairly high and very high for the thin gypsum plates. The low first resonance frequency shows that the plates can possibly be modelled as subsystems as it is below the lowest frequency band investigated.

	$f_{B(thin)}$ (Hz)	$4f_{B(thin)}$ (Hz)	f_{11} (Hz)
CLT Subsystem 4	1550	6199	40
Gypsum boards subsystem 6	5960	23840	3
Gypsum boards subsystem 2	5960	23840	3

Table 5.34: The table shows the thin plate frequency limit for bending waves $f_{B(thin)}$, four times the limit $4f_{B(thin)}$ and the first resonance of the plate f_{11} (Hz for the CLT and gypsum plates.)

5.10 CLT and gypsum plates separated by a cavity filled with mineral wool and added CD profile

5.10.1 Method

This layup is similar to the previous one. It consists of a cavity filled with mineral wool and a CD profile separating two gypsum boards and a CLT plate as shown in figure 5.39. The total loss factor for the rooms are calculated from the approximated reverberation time of 2 seconds of the measurement rooms, as in equation 2.29.

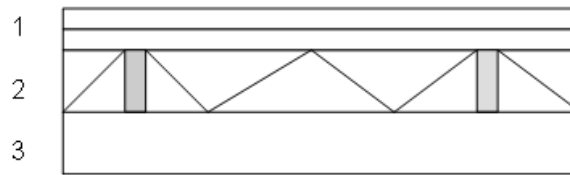


Figure 5.39:
 1) Two Gypsum boards
 2) Cavity with CD-profile and mineral wool
 3) CLT

The properties for the materials used in the layup are presented in table 5.35 and 5.31. The gypsum boards have an internal loss factor of 0,01.

	E_x in Pa	E_y in Pa	G_{xy} in (Pa)	ρ in (kg/m ³)	ν_{xy} -	ν_{yz} -
CLT	1,54e10	2,96e8	3,819e9	490	0.44	0.64
Gypsum boards	7e9	7e9	2,69e9	1200	0.3	0.3

Table 5.35: Parameter values for each part of the layup with Young's modulus in x and y direction, E_x and E_y . Shears modulus G_{xy} and Poisson's ratio for directions ν_{xy} and ν_{yz}

	ρ in kg/m ³	Flow resistivity in N s/m ⁴
Mineral wool	50 dB	60000 dB

Table 5.36: Material data for the mineral wool used in the layup with, density ρ and Flow resistivity kg/m³.

The SEA model with the appointed subsystems are presented in figure 5.40. Subsystems 1 and 5 are the sending and receiving rooms. Subsystem 2 are the two gypsum plates model as a static laminate. Subsystem 3 is the cavity with the mineral wool modelled as a trim layer. The CD profile is not included

in the cavity subsystem due to difficulties modelling it. It is instead tested as different connection between subsystem 2 and the CLT subsystem 4. The connection is not shown in the figure.

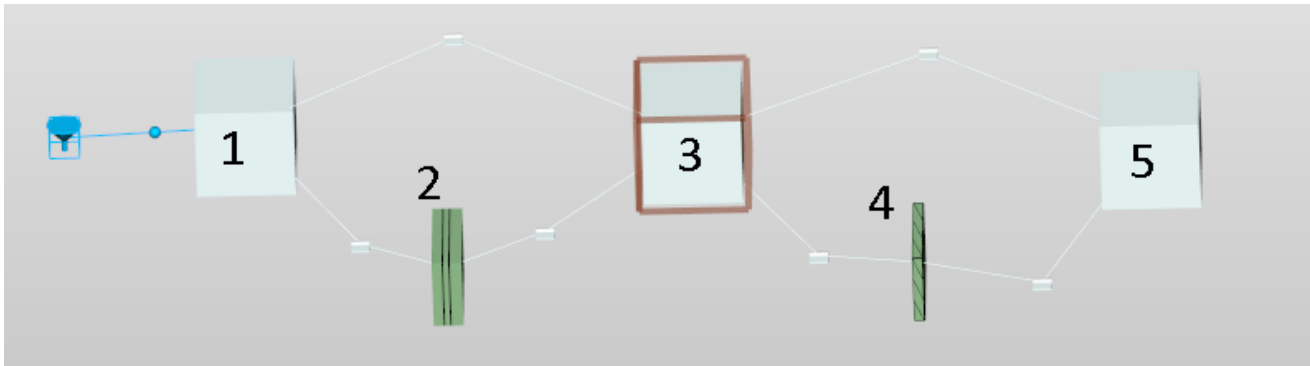


Figure 5.40: Numbered subsystems included in the SEAWOOD model.

5.10.2 Results

Figure 5.41 shows a comparison of the reduction index curves between the measurements and the SEAWOOD calculations. The different connection types refers to who the plates are coupled together and at about 200 Hz they start to differentiate a lot from each other. The line and point connection cases seems to underestimate the reduction index. When using no connection between the gypsum boards and the CLT the curves match closest to the measured data. All the cases overestimates the reduction index below 300 Hz and the no connection case only coincides with the measurement in the 300 to 800 Hz region.

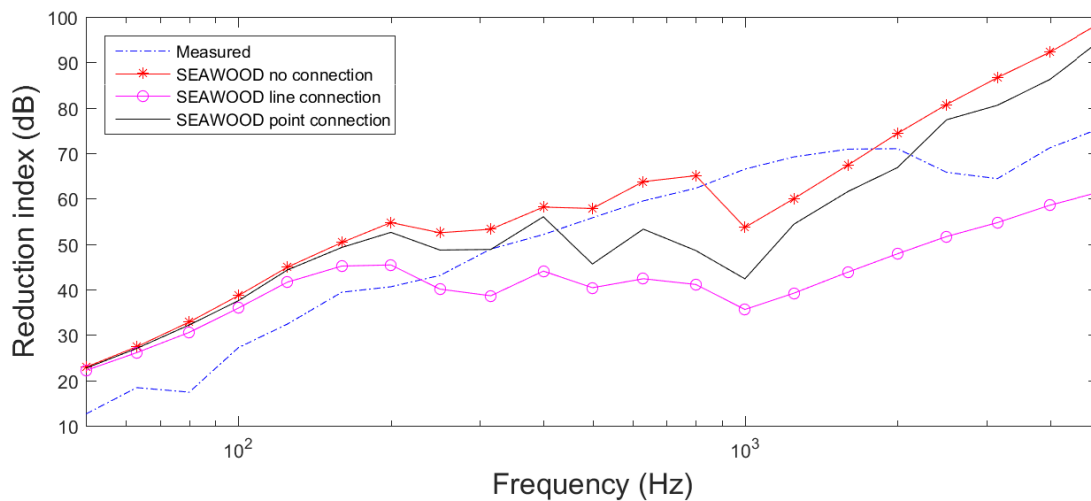


Figure 5.41: Comparison of the reduction index for SEAWOOD calculations with different plate connections and measurements

Table 5.37 shows the weighted reduction index and the spectral adaptation terms for the reduction index curves. As seen in figure 5.41 the no connection case connection type is the closest to the weighted

single values and adaptation terms for the measurements. The point connection single value reduction index is the same as the no connection case but differentiates for the spectral adaptation terms. The two curves are similar at lower frequencies and starts to coincide at 2000 Hz. The frequency in between is were they are different but not by much.

	Measured	Point connection	Line connection	No connection
R_w	55 dB	52 dB	43 dB	52 dB
C	3 dB	-2 dB	-2 dB	7 dB
$C_{50-3150}$	-9 dB	-6 dB	3 dB	-6 dB

Table 5.37: Resulting weighted reduction value R_w for third octave bands ,100-3150 Hz and the spectral adaptation terms C and $C_{50-3150}$ calculated according to ISO 717-1 [16].

The no connection case is used in figure 5.42 to investigate the direct transmission trough the cavity. The without mass law curve shows the reduction index when the direct path trough the cavity to the sending and receiving rooms is removed from the model. The figure shows precisely the expected behaviour that when removing the direct path the reduction index for the lower frequencies are increased. This suggest that the critical frequency for the layup may be at around 1000 Hz when the mass dominated regions ends.

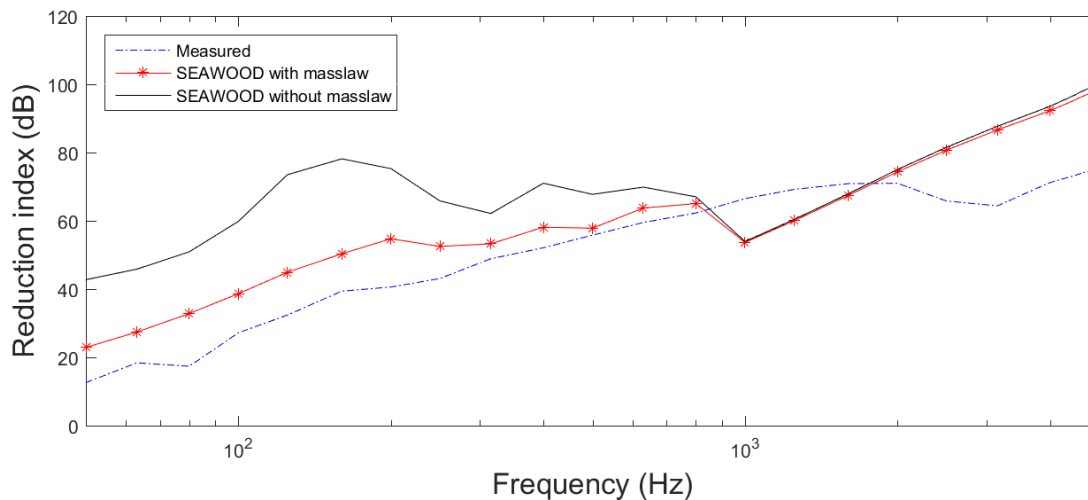


Figure 5.42: Comparisons of reduction index curves with and without direct transmission trough the cavities.

The mode count for each frequency band and the modal overlap are the same for these subsystems as in the previous layup and can be found in figure 5.38 and table 5.33. The first resonance frequency for the plates and the thin plate frequency limit for bending waves are the same as the previous layup and can be found in table 5.34.

6 Discussion

An investigation regarding the material parameters of the CLT plates were made before implementing the model into SEAWOOD. The base parameters were taken from literature sources and varied to get the best fit in the software. The different types of CLT used in the layups are in reality build from different number of layers and have different characteristics. The final material parameters used for all CLT plates are therefore not a true representation of how the plate behave in real life. The most important aspect is the internal loss factor of the plates. The CLT plates used have unnaturally low internal loss factor due to it being the best fit when using the SEA model in the software. Wood usually have a higher loss factor in the higher frequencies than the one used for the CLT plates. With this in mind, in most of the studied cases the approximated material parameters of the CLT seem to work quite well. The material parameters for the concrete Weber floor and the gypsum plate are common in literature and well documented. The insulation layers used as trim layers are however a big uncertainty. The mineral wool filled cavities have calculated loss factors depending on the mineral wool used in the trim layer.

It is important to know how the model should be divided into subsystems. The models of the layups in this thesis have been made based on studying various SEA literature. For the simpler models there are not so many approaches to take but a more experienced operator could perhaps chose differently when modelling the more advanced cases. When making the models the simpler constructions, with few plate elements or cavities, were easiest to make. The fewer subsystems included in the model made it easier to identify how the different parts contributed. When adding more elements that could be included as subsystems it became harder to properly identify what elements mattered the most to the end result. Calculation cases that included elements with material parameters that have uncertain values are also difficult to properly model. One such case is the assembly including a CLT plate and a kind of plastic foam insulation material. Some of the layups included a thin layer of plaster. These layers where not included in the models due to difficulty of finding appropriate material parameters a well as implementing them in the model. Some layups also included so called CD and CW profiles. Due to limited experience with these types of constructions the modelling may not have been optimal.

When assessing the accuracy of the SEAWOOD calculations the modal overlap and number of modes in each frequency band are important indicators. The mode count in each frequency band is suggested by literature [4] to be between 2 and 30. As stated in the theory part of this sections this is by all means not an absolute. Some of the cases with low mode count gives good results, and in other cases, with high mode count, the results are not good. The modal overlap for almost all the CLT plate cases are below one. The modal overlap is dependent on mode count as well as the damping in the system. The low number of modes in the investigated frequency range as well as the low damping in the CLT plates makes the modal overlap very low. As the CLT plates are the subsystems with the lowest modal count per band and the lowest modal overlap, the focus will lie on them. The other subsystems have better, or on some cases, similar performance. The CLT plates used in the different layups are around the same thickness and they have about the same length and width depending on the layup. Most of the CLT plates investigated in this thesis have 2 modes in the frequency band around 125 Hz but there are exceptions. The first resonance frequency of the CLT plate is in most cases lower than the investigated frequency range. The accuracy of the comparisons differ a lot between the different cases. It is hard to make the

conclusion that 2 bands per mode is enough to accurately make predictions with SEAWOOD as the contributions from the mass law calculations are in some cases as high up in frequency as 800 Hz. How much the mass law calculations contribute to the calculations differs a lot between the different cases. The mass law calculations seem to be heavily affected by how the different trim layers are modelled, as well as the material properties of these layers.

As all of the CLT plates included in the layups are around 140 mm thick it is important to find out when the assumed thin plate theory does not apply any more. The thin plate limit for bending waves has been calculated for each of the plate subsystems used in the different layups to more closely investigate this. In most cases the CLT plates have a fairly low frequency limit. It has however been suggested by Hopkins that it is possible to extend this range as much as four times the limit [11]. Thin plate theory for bending waves may accordingly be used up to $4f_{B(thin)}$ with the errors of less than 3 dB for most cases. This is usually applied to masonry and concrete but it may be applicable for the CLT plates used in the layups studied here. In most of the calculated cases the measurements and calculations coincide well above the $f_{B(thin)}$ limit which may suggest that it is possible to treat the plates as thin even at higher frequencies. In Hopkins's book he also describes that the airborne sound insulation stops to increase beyond the $4f_{B(thin)}$ limit and creates a plateau due to thickness resonances in the plate. The two single CLT plate cases studied here both shows a plateau in the higher frequencies. For the case with the CLT 140 plate in section 5.2 the calculated $4f_{B(thin)}$ frequency does not coincide with the the plateau in the measurements while the CLT 320 plate in 5.3 does. One explanation for this may be that the CLT 320 plate is much thicker than the CLT 140 plate and that the thickness resonances is more clearly shown. As these two cases are the only ones studied with just a single CLT plate it is hard to make any conclusions regarding this. It seems like the $f_{B(thin)}$ limit is not where the whole model falls apart and that $4f_{B(thin)}$ might be a more appropriate limit. It is worth noting that the quasi longitudinal phase velocity calculated for the CLT plates are using an effective value for bending stiffness due to the orthotropy of the plates. Because of this the calculated phase velocity might not be entirely accurate. As the plates used to make the subsystems are relatively thick compared to the assumed thin plate theory, the accuracy and usable frequency range of the model are depending on the plate thickness. The best case scenario would be to use thinner plates in the assemblies. This would make the calculations more reliable.

The deviations at higher frequencies may also be explained by flanking transmission problems in the lab measurements. In figure 5.15 there are two different layups being compared. They are measured in the same lab. Up until 1250 Hz there is a clear difference in reduction index but after that they start to behave very similar. Either the added gypsum does not do anything to attenuate the airborne sound or there is something else in the lab setting affecting the measurements. Another explanation for the high frequency deviations is how the CLT behaves physically. Above a certain frequency the CLT layers start to decouple from each other. This leads to an reduction of the global dynamic mass, which in turn leads to increased transmission in the high frequency region. The version of the SEA+ software used in this thesis is not able to replicate this behaviour correctly.

All the measurement data that is used came from different labs and where made by different people. The assumption is that all measurements are made correctly. Reverberation times is used to calculate the total loss factor for the sending and receiving rooms. The actual reverberation time is only given for the first three cases. For the cases with no given reverberation time an approximation was used. This may be a error source. The SEAWOOD software used to make the calculations are still under development. The software is assumed to be stable but there is always a possibility for bugs that may affect the results.

7 Conclusion

As the accuracy of the models differ a lot depending of what layup is being modelled any conclusion regarding a general frequency range where the model is valid is hard to make. All the CLT plates used in the layups suffer from a low number of modes for the third octave bands as well as low overlap. For simple models consisting of a single CLT plate with different thickness the SEAWOOD calculations seem accurate for a frequency range of about 300 to 2500 Hz for the CLT140 plate, and about 200 to 1600 Hz for the CLT320 plate. With the accuracy in the upper range depending on the thickness of the plates as well as if and when the reduction index starts to plateau. The simplified model of a CLT plate was used to determine how the software worked. Despite the poor results in the frequencies below 315 Hz there is only a few dB difference between the simplified model and the most accurate SEAWOOD calculation. This would suggest that even with a limited approach a single CLT plate can successfully be modelled in SEA.

For the simple case with a Weber concrete plate and a CLT140 plate the calculations compare very well to the measurements between 50 and 4000 Hz. The first resonate mode for both the concrete and CLT are at 51 and 56 Hz, below which it is not possible to consider the plates as subsystems. The combination of the low mode count and the low modal overlap, probably makes the good agreement in lower frequencies a coincidence. A more probable lower frequency limit would be at 200 Hz where both subsystems have at least 2 modes per band. It is also important to have in mind the corrected loss factor for the concrete Weber plate. With this said the frequency range where SEAWOOD calculations seems accurate for this type of model is 200 to 4000 Hz.

For the case with a cavity and two CLT plates as well as added gypsum, the SEAWOOD calculations seem to be accurate from about 125 to 1250 Hz where the measured curve starts to form a plateau. In the case with just a cavity and two CLT plates the SEAWOOD calculations seem fairly accurate between 100 and 1250 Hz even though the calculations undervalue the reduction index. During modelling it became clear that further study of how the mineral wool trim layer in the cavities affects the results is needed to create a more realistic model.

For the case with a single CLT plate with added plastic foam insulation the SEAWOOD calculations do not align well with the measurements. As the SEA model for a single CLT plate works quite well the deviations in this case is most likely due to incorrect material parameters of the plastic foam insulation. The layup also included a thin layer of silicone plaster that was omitted in the model, which may also contribute to the deviations. A similar case also include this foam insulation but there is also a mineral wool filled cavity and gypsum plates added. Here the SEAWOOD calculations align, for some frequency bands, with the measurement but as the material parameters for the plastic foam insulation is not trustworthy this might be a coincidence.

The next case also includes the gypsum, CLT and mineral filled cavity, but there are fixed wooden studs in the cavity as well as a layer of mineral wool insulation on the CLT plate. The SEA wood calculations overestimate the reduction index for all frequencies up until 2000 Hz. This is likely due to the damping of the mineral wool being modelled incorrectly. The wooden studs are not included from

the model and may contribute to the overestimation by omitting the coupling between the gypsum and CLT plates through the cavity. More investigation would be needed to properly model the studs included in cavities.

The last two cases are similar. The larger constitution includes a cavity containing a CW-profile and mineral wool insulation as well as another layer of two combined gypsum boards. Different types of connections between the plates was used to try to figure out how the CW and CD profiles coupled the plates together. The different connection types between the plates used in the model are very different in the two cases. In the larger case the best result was given by using point connections between the plates. Even though the reduction index and weighted reduction index corresponds well to the measurement the large difference between the different connection types suggest that this is a coincidence. In the smaller construction case the line connection type gave the best result. Again there is a large difference between the different connection types even though the line connection compares well to the measurement. The different results from these approaches makes it hard to draw any conclusions regarding the connection types. These models need to be approached in a different way and a better implementation of the CD and CW profile is needed.

From these results it seems that SEAWOOD can calculate the reduction index of simple layups including CLT plates quite well. There are however a few things that need to be considered. A closer investigation of the high frequency deviations are needed to make the model more accurate. There is also a need to find better material parameters to include in the model as well as more appropriate internal loss factors. For the more complicated layups a better way to implement them in SEAWOOD is required. Traditional SEA theory is based on the coupling of the resonate modes of the subsystems. As both the mode count and modal overlap increases with frequency, SEA is best suited to make accurate prediction for higher frequencies. Most of the plates included in the assemblies studied in this thesis have both low mode count and low modal overlap. A suggested minimal number of modes in each third octave band was found in literature to be 2 to 30. The limit of the 30 modes per band is not reached for most of the plates until 3000 or 4000 Hz. The plates included as subsystems have 2 modes in each frequency band beginning at around 200 Hz. The upper frequency limit for thin plates depends on the thickness of the plates included in the construction. Most of the plates used in the study have a $4f_{B(thin)}$ limit at around 5000 Hz but for some plates this limit increases above the studied frequency range. For some of the thicker plates this limit is instead around 3000 Hz. But as the $4f_{B(thin)}$ limit is not a definitive limit the results might still be valid above those frequencies. If 2 modes per frequency band can be accepted as a lower limit, the general frequency range that the SEA approach is valid for these types of constructions is about 200 to 5000 Hz. This is very important to have in mind when drawing any conclusions regarding the accuracy of the models. Even though the result seems very promising for some of the cases, the trouble with the low mode count and modal overlap in the whole investigated frequency region makes it so that the result cannot be fully trusted. The lower frequency region limitations of SEA suggests that another method would be more appropriate to use when investigating those frequencies.

Bibliography

- [1] R. H. Lyon and R. G. DeJong, *Theory and application of statistical energy analysis*, Second Edition. Newton: Butterworth-Heinemann, 1995 (cit. on p. 3).
- [2] J. F. Chalmers, “Building acoustics and community noise(bac)”, Lecture notes, VTA 125, 2013 (cit. on pp. 4, 11).
- [3] T. E. Vigran, *Building Acoustics*. New York: Taylor and Francis, 2008 (cit. on pp. 4, 9, 11).
- [4] R. J. Craik, *Sound transmission Through buildings: Using statistical energy analysis*. Old post Road, Brookfield, Vermont 05036, USA: Gower, 1996 (cit. on pp. 5, 6, 8, 9, 64).
- [5] K. Tageman, “Modelling of sound transmission through multilayered elements using the transfer matrix method”, Master’s thesis, Chalmers University of Technology, Division of Applied Acoustics, 2013 (cit. on pp. 5, 11).
- [6] I. AC, “Sea+ advanced theory”, Verison 2014-3, 2014 (cit. on pp. 5, 10, 11, 13).
- [7] —, “Sea+, sea+ lite version seawood, user’s guide”, Verison 2014-5, 2014 (cit. on p. 11).
- [8] —, “Sea-foam theory”, Verison 2014-1, 2014 (cit. on p. 11).
- [9] C. G. M. Villot and L. Gagliardini, “Predicting the acoustical radiation of finite size multi-layered structures by applying spatial windowing on infinite structures”, *Journal of Sound and Vibration*, vol. 245(3), 2001 (cit. on p. 13).
- [10] G. Borello, “Training to sea and seawood software”, InterAC, 2015 (cit. on p. 14).
- [11] C. Hopkins, *Sound Insulation*, First edition. Linacre House Jordan Hill Oxford OX2 8DP UK: Elsevier Ltd, 2007 (cit. on pp. 15, 16, 19, 25, 65).
- [12] J. E. Reinhard Stürzenbecher Karin Hofstetter, “Cross laminated timber: A multi-layer, shear compliant plate and its mechanical behavior”, Vienna University of Technology, Tech. Rep., 2010 (cit. on pp. 19, 22, 23).
- [13] H. G. E. Simon Aicher H.W. Reinhardt, *Material and Joints in Timber Structures*, Volume 9. Springer Dordrecht Heidelberg New York London: Springer, 2014 (cit. on pp. 19, 22, 23).
- [14] S. Enso, “Stora enso building and living. building solutions”, Stora Enso, Tech. Rep., 2012 (cit. on pp. 1, 19, 25).
- [15] Y. H. C. Qinyi Zhou Meng Gong and M. Mohammad, “Measurement of rolling shear modulus and strength of cross laminated timber fabricated with black spruce”, *Construction and Building Materials*, 2014 (cit. on pp. 19, 20).
- [16] ISO-717-1:1996(E), *Acoustics -rating of sound insulation in buildings and of building elements-part1: Airborne sound insulation*, INTERNATIONAL ORGANIZATION FOR STANDARDIZATION, 1996 (cit. on pp. 27, 31, 35, 39, 40, 44, 48, 53, 58, 63).
- [17] K. Bodlund, “Luftljudsisolering. en sammanställning av tillämplig teori”, Byggeforskarrådet, Tech. Rep., 1980 (cit. on p. 33).
- [18] W. Kropp, “Technical acoustics 1, propagation and radiation of structure borne sound”, Lecture notes, 2015 (cit. on p. 37).

A Appendix

Edit MW Impact Sound 20mm (Porous Material)

Name
MW Impact Sound 20mm

Properties
Model: FOAM (6 dofs)
Generic Fluid: Air

Density	184 kg/m ³	Young's Modulus	5200000 Pa
Flow Resistivity	68000 N s/m ⁴	Shear Modulus	5200000 Pa
Porosity	0,99	Poisson's Ratio	0,1
Tortuosity	1,7	Viscous Length	8E-05 m
Loss Factor	0,1	Thermal Length	0,00016 m
Compression Rate	1	Compression Type	1D
Fiber Diameter	1,5E-05 m		

User Notes

OK Cancel

Figure A.1: Full material data for the impact sound insulation layer used in SEAWOOD modelling.

Edit Plastic foam (Porous Material) ✕

Name

Plastic foam

Properties

Model: FOAM (6 dofs)

Generic Fluid: Air

Density	<input type="text" value="31"/> kg/m ³	Young's Modulus	<input type="text" value="143000"/> Pa
Flow Resistivity	<input type="text" value="87000"/> N s/m ⁴	Shear Modulus	<input type="text" value="2,3E+07"/> Pa
Porosity	<input type="text" value="0,97"/>	Poisson's Ratio	<input type="text" value="0,3"/>
Tortuosity	<input type="text" value="2,52"/>	Viscous Length	<input type="text" value="3,7E-05"/> m
Loss Factor	<input type="text" value="0,055"/>	Thermal Length	<input type="text" value="0,000119"/> m
Compression Rate	<input type="text" value="1"/>	Compression Type	<input type="text" value="1D"/>
Fiber Diameter	<input type="text" value="1,5E-05"/> m		

User Notes

Figure A.2: Full material data for the plastic foam layer used in SEAWOOD modelling.